(2)

Joining Alumina to Sapphire for Copper Vapor Laser Tubes

Antoni P. Tomsia, Andreas M. Glaeser and Joseph A. Pask

Pask Research & Engineering, Inc.
1022 Francisca Ct.
Pinole, CA 94564

Final Report
Contract No. N61331-90-C-0005

Work performed form February 20, 1990 to August 20, 1990

Prepared for

Naval Coastal Systems Center
Code 7523
Panama City, Florida 32407-5000

Unclassified/unlimited

September 10, 1990

The views, opinions and/or findings contained in the report are those of the author's and should not be construed as an official Department of the Navy position, policy, or decision, unless so designated by other documents

Introduction:

Project Overview:

The technology for building copper vapor lasers has existed for years. The joining technology for producing sealed copper vapor lasers did not. Thus, our focus during Phase I research was to explore means of joining alumina to alumina and alumina to sapphire for high temperature applications. We felt that it was imperative to explore more than one joining technique, and for a given technique, to investigate a range of conditions or compositions, or both.

The motivation for this approach was twofold. First, it was beyond the scope of Phase I research to exhaustively explore the mechanical and chemical stability of all joints produced by a broad assortment of joining techniques, particularly for the timeframes of interest for a sealed copper vapor laser. We recognized that joining methods that produced bonds of adequate quality to survive limited thermal cycling and limited exposure to copper might prove to be inadequate for long-term use. Thus, if the method that appeared most satisfactory in Phase I testing proved inadequate for fabrication of sealed copper vapor lasers, we would have the needed experience with alternative joining approaches to adjust and adapt rapidly. Second, we felt that it was possible that more than one joining approach would be suitable, and that it might be advantageous to use more than one joining method in producing the total system. Those who had chosen to explore only one joining method would lack this flexibility.

As a result of this research philosophy, four approaches to joining sapphire to alumina were explored: 1) solid-state or **direct** joining, 2) use of glass-bonded alumina interlayers, 3) joining with a devitrifiable **glass**, and 4) use of a **metallic** (Nb or Pt or their alloys) interlayer. Extensive microstructural and microchemical characterization of joint interfaces was performed to assess the quality of the bonds produced. For selected samples, bend beams could be produced, and four-point bend strength was determined. For samples bonded with metallic interlayers, chemical compatibility of the interlayer with copper was investigated. Successfully bonded samples were subjected to thermal cycling to assess the thermal shock resistance of the bonded interfaces. Collectively, these results indicate the relative strengths and weaknesses of the four approaches. This information, in conjunction with an assessment of the relative ease of applying these techniques to (larger-scale) copper vapor laser systems, establishes the joining approaches that merit further investigation during Phase II. Since long-term containment of copper vapor and sustained laser operation are the goals of sealed-tube technology, Phase II research would also address the critical issues of long-term microstructural, thermomechanical and thermochemical stability. Thus, the objective of Phase II work would be to refine and adapt these methods to the cost-effective fabrication of sealed tubes.

This report contains several sections. First, we review some of the characteristics of the competing joining technologies for the fabrication of sealed copper vapor lasers. The results of our work are presented in four major sections, corresponding to the four joining approaches that were explored. Finally, the results of the entire Phase I program are summarized.

Competitive Joining Approaches:

The role of ceramics in engineering is changing rapidly. New uses of ceramics as structural or electronic materials are being developed or considered. Many promising applications for ceramics require that a complex or large assembly be fabricated by joining simpler and/or smaller components. In many cases, different ceramics must be joined, or a ceramic must be bonded to a metal alloy. Successful utilization of ceramics for these applications requires reliable joining techniques. Joining is a key enabling technology [1]. Contributions to the technology are

likely to have a broader, long-term, beneficial impact. This also impacted our decision to explore a broad range of joining methods.

Viable joining techniques must form a strong bond, and should cause minimal degradation of the base material(s). Successful sealing produces bonds that are : 1) strong, 2) reliable, and 3) relatively inexpensive to manufacture. It is therefore of critical importance to identify and understand the processing conditions (materials chemistry, interfacial reactions, temperature, time, pressure, etc.) which lead to the formation of strong, reliable, and economical bonds/joints.

In most methods for bonding metals to a ceramic (and by extension a ceramic to a ceramic via a metallic interlayer), the procedures are limited to a particular pair or set of materials which are chemically compatible, and for which thermal expansions are closely matched. These techniques are usually based on the brazing principle, in which a liquid metal (or a glass) wets and usually reacts at the interface, forming the bond. One of the attractive features of these approaches is that surfaces need not be polished; the liquid fills any irregularities. However, as normally nonreactive metals do not wet oxide ceramics, these techniques are restricted in application. Since titanium-containing alloys normally react with ceramics, they are most commonly used for forming bonds. However, the bonds are designed for components operating at or near ambient temperature. If a glass, rather than a metal, is used, wetting of the ceramic normally occurs. However, to facilitate sealing, the glasses often have a relatively low softening temperature. Unless dissolution and incorporation of the ceramic(s) in the glass raise the softening temperature, these bonds also have limited temperature capability.

In some cases, techniques have been developed to metallize the ceramic surface prior to electrodeposition and/or conventional brazing; usually gold or silver alloys are used. Elaborate preparative and sealing procedures are usually involved, requiring the use of active or inert gas atmospheres during all stages of processing. Perhaps the most serious limitation to a more widespread use of the above-mentioned techniques is the restricted temperature capability of the resulting bonds.

Sealed CVLs provide a number of challenging constraints and requirements. Both the system and the bond must withstand prolonged operation (most likely thousands of hours) at high temperature (about 1500°C) without deleterious chemical interaction or mechanical degradation. The high operating temperature is necessary to provide an adequate copper vapor pressure, but the presence of copper creates the possibility of long-term chemical interactions with the bond if metals or glasses are used. Occasional shutdown of the system due to failure or instability of the electronics is almost inevitable, and thus the system must be designed to withstand at least a limited number of thermal cycles. This imposes stringent constraints upon the maximum allowable thermal expansion mismatch. The thermal expansion anisotropy of sapphire provides a further complication.

It is our experience that there is no detrimental long-term chemical interaction between (glass-free) alumina and copper in CVLs. Thus, a direct bond between sapphire and alumina should not undergo chemical degradation. We have previous experience with **direct bonding** of sapphire to polycrystalline alumina, and had generated small continuously bonded sapphire-alumina interfaces [2,3]. There is, however, a thermal expansion mismatch between polycrystalline alumina and c-axis sapphire. Although we had been able to thermally cycle small bonded specimens between room temperature and 1600°C without cracking, the applicability of this approach to samples having the dimensions and geometries of typical laser tubes and sapphire windows had not been demonstrated. Thus, ease of fabrication and thermal expansion mismatch induced failure were potential obstacles to utilization of this approach.

An alternative approach to joining sapphire to alumina entails the use of **metal** interlayers in conjunction with solid-state bonding. Methods for the direct solid-state (reaction) bonding of

metals to ceramics are described in the literature [4,5]. Bonds formed using these methods do not have the same temperature limitations as the techniques mentioned previously. They are characterized by adequate mechanical strength and leak tightness at moderate to high temperatures, very often at temperatures approaching those at which the bonds were formed.

Solid state reaction bonding procedures are simple and have the following characteristics:

- Bonding temperatures lie below the melting point of the lowest melting component in the system (generally the metal or alloy) - usually about 90% of the melting point in degrees absolute.
- Usually an air atmosphere is used for bond formation, but argon or vacuum can also be used when necessary.
- Light clamping pressures are used, sufficient to ensure good physical contact at the interface during bonding (0.5-1.5 MPa).
- Bonding times vary from a few seconds to as much as several hours.
- The surface of the ceramic to be bonded must be polished to a finish approaching optical flatness for maximum bond strength.

An account of the influence of the above factors on bond formation between several metals and alumina has been published [6,7].

However, there are obstacles to applying this approach to CVL systems. Although sapphire windows can be polished to a high quality finish, it is uncertain whether the appropriate alumina tube surfaces can be given a sufficiently high quality finish. Furthermore, if the sealed laser tubes are large, controlled atmosphere furnaces and clamping systems capable of accommodating such large tubes of this length will be required. In all cases, long-term high temperature thermochemical compatibility between the interlayer and alumina, sapphire, and the copper vapor is required, and may be difficult to achieve.

Two other approaches entail the development and use of glass-bonded **alumina interlayers** and sufficiently refractory glass frits (**glass interlayers**) to join ceramics or ceramics to metals. Provided the layers have a sufficiently low viscosity at the joining temperature, little or no externally applied pressure may be required to induce flow, and thus, the quality of the surface finish may be less critical. The interlayers, being primarily alumina have good thermal expansion match with pure alumina; for the glasses, the thermal expansion coefficient can be adjusted to reduce thermal expansion mismatch. Long-term high temperature thermochemical compatibility between the interlayer and alumina, sapphire, and the copper vapor remains a requirement.

Our initial assessment indicated that each method of joining had strengths and limitations. The Phase I research was designed to test these four methods of joining alumina to sapphire: 1) solid-state or **direct** joining, 2) joining with glass-bonded alumina interlayers, 3) joining with a devitrifiable **glass**, and 4) use of a **metallic** (Nb or Pt alloy) interlayer, and to identify the joining method(s) and processing conditions that produce strong, reliable bonds best satisfying the additional requirements and constraints imposed upon a sealed CVL system. The ensuing sections describe this research. Where appropriate, results from independent research assessing the extension of these methods to joining of alumina to alumina are included.

Phase I Research Results:

I. Direct Joining of Alumina to Sapphire:

Introduction

The first approach tested was the direct bonding of sapphire to alumina. Conditions for producing continuously bonded interfaces utilizing this method had already been defined [2,3]. Small bonded samples (several mm by several mm) had been thermally cycled between room temperature and 1600°C without failure. The major unresolved questions were whether or not this method could be scaled up to dimensions characteristic of laser tubes and sapphire windows, and whether or not the larger specimens would survive thermal cycling. To address these issues, we produced a larger (1" × 1") continuously bonded sapphire/alumina sample and conducted thermal cycling experiments.

Experimental Procedures:

Materials

The alumina used for the tests was manufactured by Coors, and is 99.5‰ alumina with the balance MgO and glass. The material was received in the form of large 3 mm thick plates which were cut into ≈22 mm × 22 mm plates. For these experiments, the plates were polished using progressively finer grit diamond paste and vibratory polishers to produce a 1 μm finish. Polishing took approximately three weeks.

Randomly oriented high-purity sapphire single-crystal wafers were purchased from Meller Optics (Providence, Rhode Island). The sapphire wafers were cut to the same ≈22 mm × 22 mm × 3 mm dimensions; the wafers are polished to a 0.25 μm finish by the vendor, and were used without additional polishing. Prior to hot pressing, the samples were cleaned using organic solvents and annealed for 2 h in air at 1200°C to remove any organic contaminants from the surface.

Hot Pressing Conditions

A sapphire/alumina ensemble was placed in a high-purity graphite die. Grafoil™ sheets were placed between the ensemble and the die pistons to accommodate any misalignment. The die was loaded into a vacuum hot press. The system was evacuated until a vacuum of $<5 \times 10^{-6}$ torr was attained. A load sufficient to produce a bonding stress of 15 MPa was then applied and maintained throughout the remainder of the bonding. The press was heated at 10°C/min to a pressing temperature of 1400°C. The ensemble was held at this temperature for 12 h. The sample was then cooled at ≈10°C/min to 500°C, isothermally annealed at 500°C for 2 h, and then cooled at 10°C/min to room temperature. The applied load was then released.

Interfacial Characterization

The ensemble was cut approximately in half using a diamond wafering saw. The sections were mounted and diamond polished to a 1 μm finish. Polished samples were examined using both optical and scanning electron microscopy. Complete cross sections were examined to determine the quality of the bond that was produced.

Results and Discussion

The combined effects of a high quality surface finish, an extremely flat surface, and relatively high bonding pressure produced excellent quality joints. There is an abrupt transition from the pore-free sapphire (Figure I-1a, top) to the incompletely densified alumina (Figure I-1a,bottom). However, in contrast to some of the interfacial microstructures observed in other joining studies (see Section II - Joining with Glass-bonded Alumina Interlayers), there are few if any residual cracklike defects that mark the original position of the sapphire/alumina interface. The portion of the interface shown in Figure 1b illustrates one of the **most** serious imperfections found.

Bonded samples were subjected to thermal cycling. Die penetration and optical microscopy were used to test the integrity of bonds before and after cycling. Samples were heated in a furnace to 1550°C, and the temperature was allowed to decrease to 800°C as rapidly as the thermal characteristics of the furnace would permit (≈50-60°C/min initially). When the temperature reached 800°C, the temperature decrease was halted, and the sample was heated in 60 min to 1550°C. After five thermal cycles between 800°C and 1550°C, no degradation in bond quality was observed.

The results are encouraging. Although it may not be practical to join large components by hot pressing, the results do indicate that with proper care given to surface preparation and the imposition of a sufficiently high load, a high-purity alumina and sapphire can be joined effectively by means of direct bonding. The same should apply to joining of high-purity aluminas to one another. If glass-bonded interlayers are used, the glassy phase should facilitate flow, and reduce the demands on surface preparation somewhat compared to direct bonding of alumina to sapphire.

Summary

Sapphire has been bonded to 99.5‰ alumina by vacuum hot pressing (1400°C, 15 MPa, 12 h, $<5 \times 10^{-6}$ torr). By using samples with flat polished surfaces, a sapphire/alumina interface that is essentially free of bonding defects was produced. Five thermal cycles between 800°C and 1550°C produced no observable degradation in bond quality.

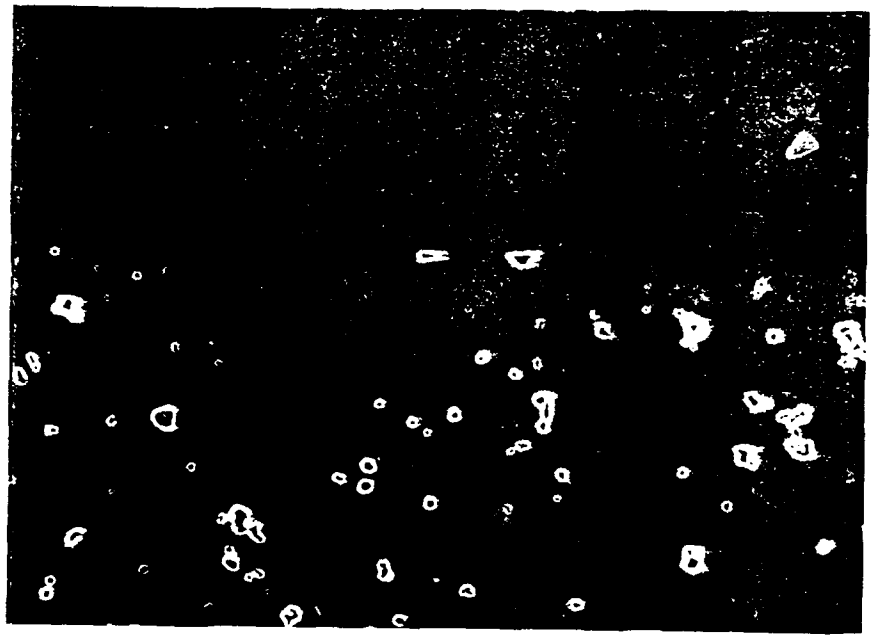

50 μm

25 μm

Figure I-1 a) Lower magnification (500×) and b) higher magnification (1000×) SEM micrographs of interface between 99.5‰ alumina and sapphire produced by hot pressing.

II. Joining With Glass-Bonded Alumina Interlayers:

Introduction

The use of glass-bonded alumina interlayers to join nominally glass-free aluminas represents a compromise between joining with glasses and direct bonding. There are several advantages to using glass-bonded interlayers. Principal among these is that creep/flow of the interlayer may ease otherwise stringent requirements imposed on surface flatness. Other advantages are an inherently good thermal expansion match with alumina and the ability to use the bonded assembly in air. If the glass is equilibrated with the alumina, no deleterious *chemical* reactions between the glass and alumina should occur. *Microstructural* degradation is a concern, and long-term degradation will need to be assessed.

This section of the report describes the results of our investigation of the use of glass-bonded alumina for joining alumina to sapphire. Results from an independent study of the suitability of the approach for joining alumina-to-alumina are incorporated. The comparison provides an indication of the relative importance of surface finish and flatness on the quality of the joined assemblies, and the impact of microstructural changes at the interface on the morphological evolution of interfacial defects. The general objective of the study was to determine the relative importance of several processing parameters on bond quality, and thereby to define directions for future research.

Experimental Procedure

Three different grades of alumina and sapphire single-crystal wafers were assembled in various ways to produce interfaces between a range of alumina-rich materials of differing purity and with differing levels of surface preparation. The materials, assembly configurations, bonding conditions, and methods of interfacial characterization are described in the following sections.

Materials

Three aluminas, all manufactured by Coors, were used. The aluminas spanned a relatively broad range of purity – 95‰ alumina (5‰ glass), 99.5‰ alumina, and 99.8‰ alumina. The higher purity aluminas generally contain minor amounts of magnesia as a sintering aid, and almost invariably contain small amounts of glassy phase. Randomly oriented high-purity sapphire single-crystal wafers were purchased from Meller Optics (Providence, Rhode Island).

The as-received 99.5‰ and 99.8‰ aluminas were cut into plates ≈22 mm × 22 mm × 3 mm from larger 3 mm thick plates. Polished (6 μm finish) and as-received plates of the higher-purity aluminas were prepared. The 95‰ alumina plates were ≈0.6 mm thick and cut to form ≈22 mm × 22 mm plates. Attempts to polish the 95‰ alumina plates were unsuccessful. The plates were not flat, and very difficult to handle because they were so thin. As a result, these plates were left unpolished. High-purity sapphire wafers were cut to the same ≈22 mm × 22 mm × 3 mm dimensions; the wafers are polished to a 0.25 μm finish by the vendor, and were used without additional surface preparation.

Assemblies and Bonding Conditions

Three assemblies using different grades of alumina and testing the effects of surface preparation were produced. The sample designations indicate the purity and surface preparation. The materials are indicated as 95, 995, 998, and S. Unpolished surfaces are indicated by the symbol U, polished surfaces by the symbol P. Thus, a sandwich consisting of 99.8‰ alumina with unpolished surfaces with an intermediate layer of 95‰ alumina (which was unpolished in all experiments described in this section) is designated as 998U/95/998U (also A-1). This was one of

the configurations tested. Two additional configurations, designated 998P/95/995P (A-2) and 998U/95/995P (A-4) were tested to assess the effect of polishing the aluminas, and to study the effect of alumina composition on joint quality. Two additional configurations utilizing sapphire and designated 998P/95/S were prepared and examined; these configurations are referred to as A-3 and A-5. The sample configuration information is also presented in Table I.

TABLE I: Sample configurations tested

Sample Code	Designation	Description
A-1	998U/95/998U	998 unpolished/95/unpolished 998
A-2	998P/95/995P	998 polished/95/polished 995
A-3	998P/95/S	998 polished/95/sapphire
A-4	998U/95/995P	998 unpolished/95/polished 995
A-5	998P/95/S	998 polished/95/sapphire

For bonding, ensembles were heated at 10°C/min to a temperature of either 1600°C (samples A-1, A-2, and A-3) or 1700°C (samples A-4 and A-5) in a 5×10^{-6} torr vacuum under a 300 g applied load. This load produces an applied stress of less than 1 psi, and is used to simulate the load that would be applied to an interface by the weight of a larger sample. Samples were held for 2 h at the bonding temperature. Subsequently, samples were cooled to room temperature at 10°C/min.

Interfacial Characterization

Samples were cut approximately in half using a diamond wafering saw. The sections were mounted and diamond polished to a 1 μm finish. Polished samples were examined using both optical and scanning electron microscopy. Complete cross sections were examined. The degree of bonding defined as the fraction of the total interfacial length along which bonding was apparent was determined from several micrographs for each interface. Samples were also etched to assess the microstructure at and adjacent to the bond interfaces.

Results

All of the samples that were prepared bonded to some extent. None of the ensembles separated during removal from the furnace, or during subsequent handling. The degree of bonding in random cross sections varied from a low of <5‰ to a high of ≈100‰. In some of the more highly bonded samples, the degree of bonding was nonuniform along the interface. More detailed descriptions and micrographs of the interfaces follow.

Alumina to Alumina Bonding Studies

Sample A-1 (998U/95/998U): This sample, which was bonded at 1600°C, had a poor quality bond. Although the sample held together, the cross section examined showed <5‰ of the interface was bonded. Along most of the interface, the mounting resin had infiltrated the alumina/alumina interfaces, as illustrated in Figures II-1a and II-1b. Regions in which there was bonding, as illustrated in Figure II-2, were the exception. The 95‰ alumina plates polished nonuniformly, suggesting that they are not flat.[1] This can produce large gaps between the

1 Plates polished for two weeks on vibratory polishers were only partially polished and showed large unpolished regions. With thicker plates, a surface grinding step can be used to improve the initial flatness.

adjoining surfaces. The results suggest that at 1600°C, the very modest applied load produces inadequate flow of the glass-bonded alumina to close the interfacial gaps.

These results, negative though they are, have important ramifications. They indicate surface preparation will be very important if bonding is to be conducted at 1600°C at the stress used. Either flatter, possibly smoother surfaces, a higher bonding temperature, a higher bonding stress, or a less refractory interlayer will be required to promote intimate contact. Comparatively, bonding with glasses will be much less demanding than bonding with glass-bonded alumina interlayers; direct bonding of high-purity alumina to high-purity alumina will be even more demanding.

250 μm

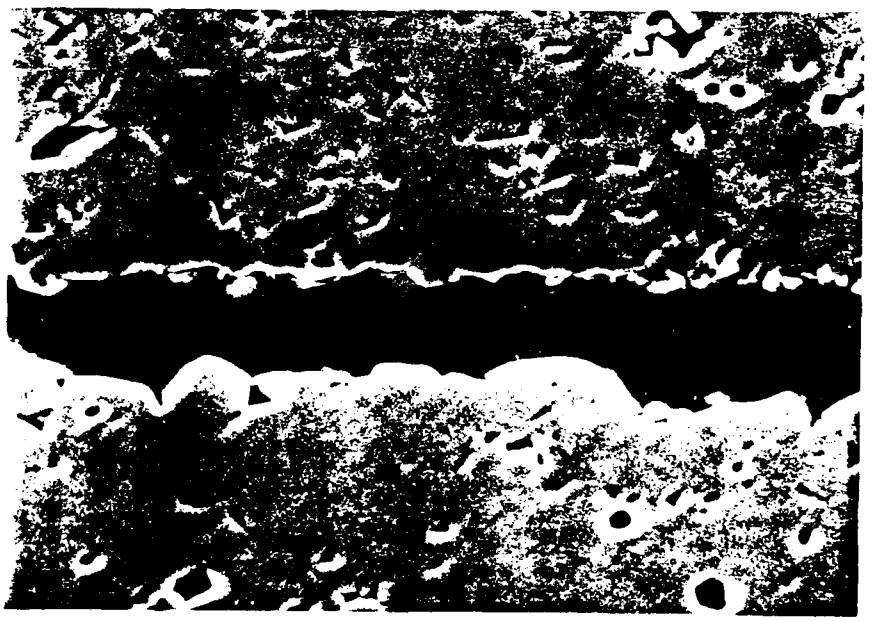

25 μm

Figure II-1 a) Low magnification, and b) high magnification SEM micrographs of interfaces in Sample A-1 illustrating poor bonding.

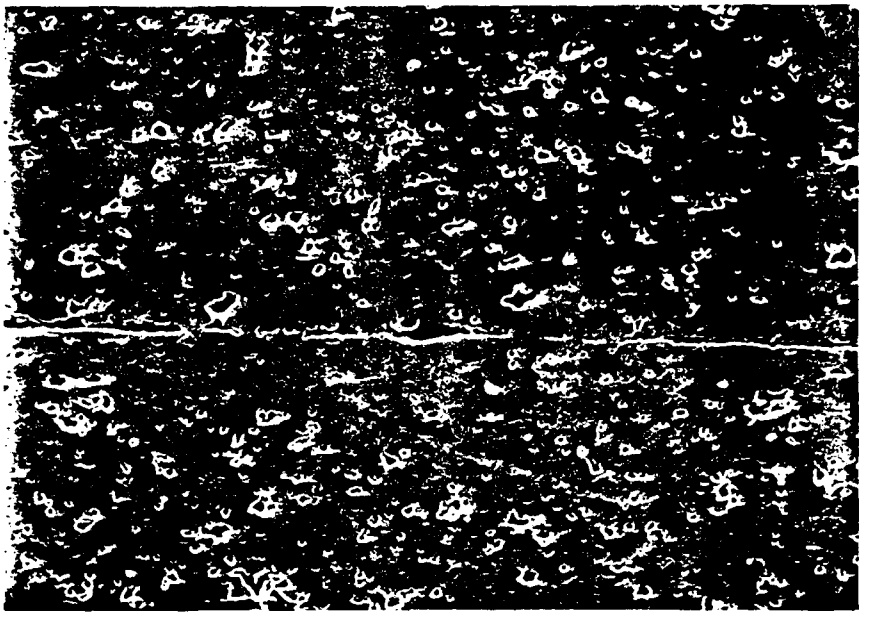

Figure II-2 SEM micrograph of interface between 95‰ glass-bonded alumina and 99.8‰ alumina.

Sample A-2 (998P/95/995P): The objective in this experiment was to assess the effect of polishing the more rigid of the components, the higher-purity aluminas, and simultaneously, to compare the bonding characteristics of two slightly different grades of alumina at 1600°C.

Examples of the interfacial structure and bond quality for the two interfaces are provided in Figure II-3. The results suggest that there is some benefit from polishing. For the *998P/95* interface, ≈33 ± 13‰ of the interface was bonded.[2] For the *95/995P* the corresponding value was 30 ± 11‰. Although this represents a substantial improvement over the results for sample A-1, substantial portions of the interface remain unbonded, and the large unbonded segments at the interface are likely to facilitate failure along the interface. As a result, additional steps to improve the quality of the interface were pursued.

---

2 In each case, several micrographs, each spanning ≈230 μm of the interface were examined, and the ‰ bonding in each micrograph was measured. The measurements from several micrographs were then averaged, and the standard deviation determined.

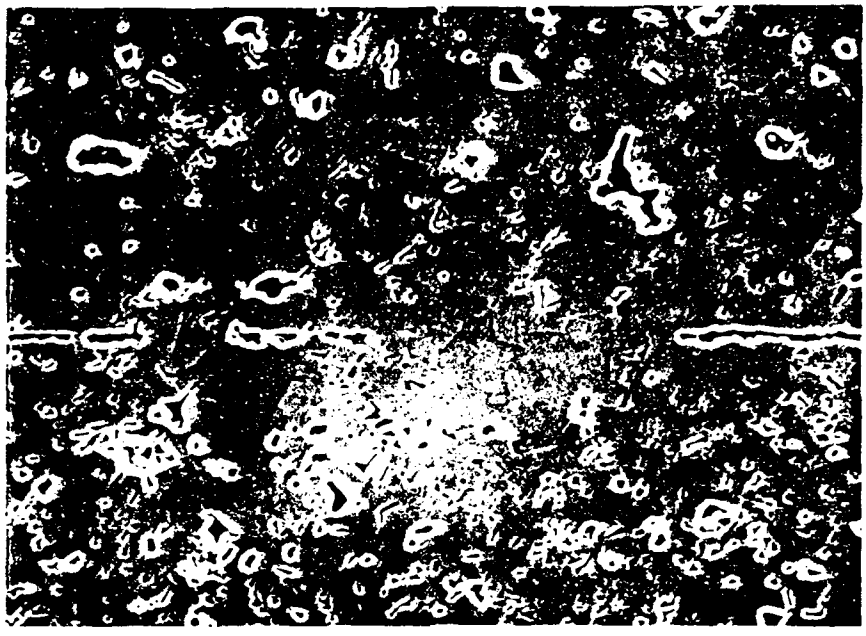

50 μm

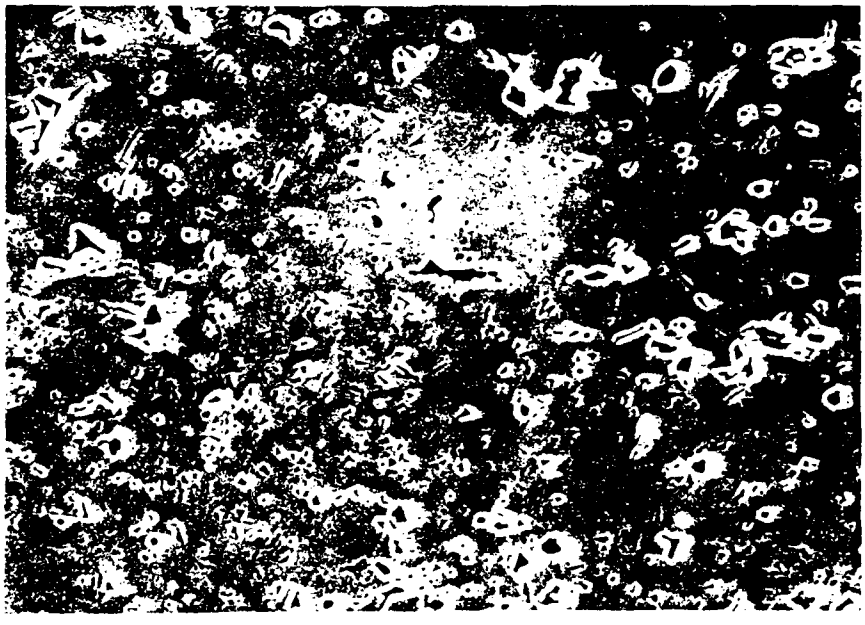

50 μm

Figure II-3 SEM micrographs of interface between glass-bonded 95‰ alumina and a) 99.5‰ alumina and b) 99.8‰ alumina.

Sample A-4 (998U/95/995P): This experiment was designed to explore the effect of an increase in bonding temperature to 1700°C on the quality of the bond. The temperature dependence of the creep rate for the specific glass-bonded alumina used was not measured. However, a 100°C increase in bonding temperature was expected to promote flow of the interlayer, and thereby, improve the quality of the bond. Since the polished 99.5 and 99.8‰ aluminas had nearly the same degree of bonding with 95‰ alumina after bonding at 1600°C, different surface finishes were used to see whether the degree of polish was an important factor affecting bond quality at the higher bonding temperature.

The results for the two interfaces differed substantially. For the *998U/95* interface, the degree of bonding was highly variable, but generally low. Measurements indicate that an average of only 26‰ of the interface was bonded, with a standard deviation of order 24‰; the interfacial structure is illustrated in Figure II-4a.. This result was similar to that obtained during bonding at 1600°C. In contrast, for the *95/995P* interface, 72‰ bonding was achieved in an average section, with a standard deviation of ±18‰. In some cases, it was difficult to determine the original position of the interface, as illustrated in Figure II-4b. The results suggest that polishing of the surfaces improves bond quality even at 1700°C.

Sapphire to Alumina Bonding Studies

Sample A-3 (998P/95/S): The objectives of this experiment were to assess effects of surface finish and flatness on bond quality. One would expect that the *998P/95* interface should yield a similar degree of bonding to that observed in sample A-2. The sapphire wafer is flatter than standard polished samples. Thus, if sample flatness is a limiting factor, these experiments were expected to indicate this. One complication is the potential for abnormal grain growth of the sapphire seed into alumina during bonding.

Measurements on the *998P/95* interface yielded results that were qualitatively in agreement with those of sample A-2. The interfaces was 38 ± 20‰ bonded. A better than average segment of the interface is shown in Figure II-5a. The quality of the *95/S* interface was better, with 65 ± 23‰ of the interface bonded. The seed had advanced by 10-20 μm into the glass-bonded alumina during bonding at 1600°C in those regions where the interfacial defects had healed, as illustrated in Figure II-5b. The results seem to indicate that grain boundary migration is the result of healing and not *vice versa*.[3] The results do suggest that flat surfaces are beneficial, consistent with results of other studies of diffusion bonding.

---

[3] In glass-free polycrystals, one would expect a reduction in the pore/crack coordination number to decrease the thermodynamic stability of the defect. This does not appear to be a factor here.

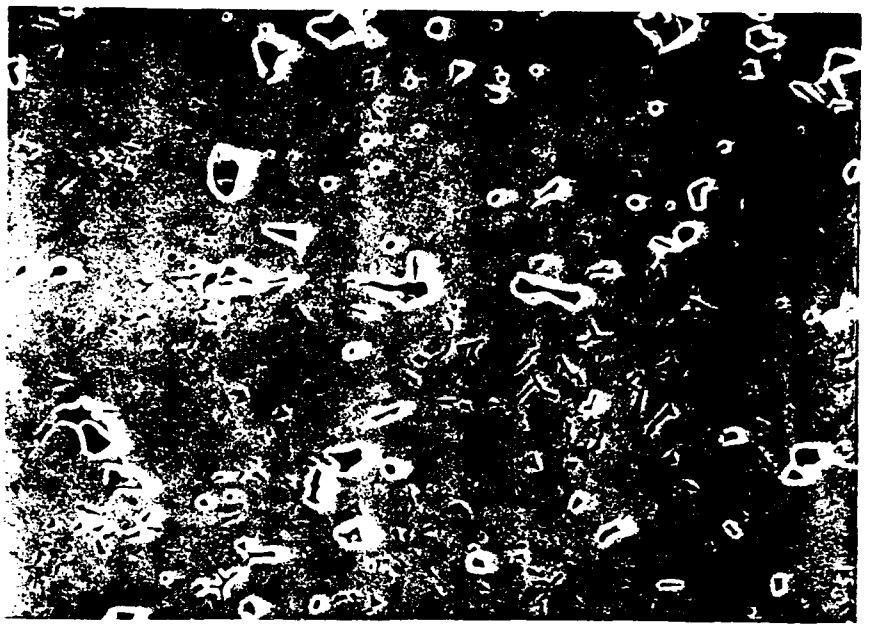

50 μm

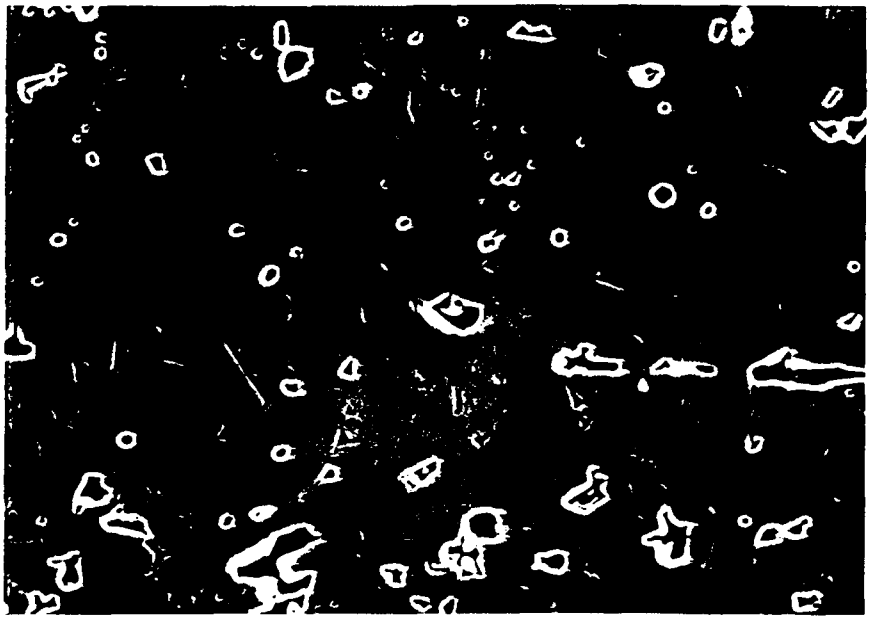

50 μm

Figure II-4 SEM micrographs of interface between glass-bonded 95‰ alumina and a) 99.8‰ alumina and b) 99.5‰ alumina.

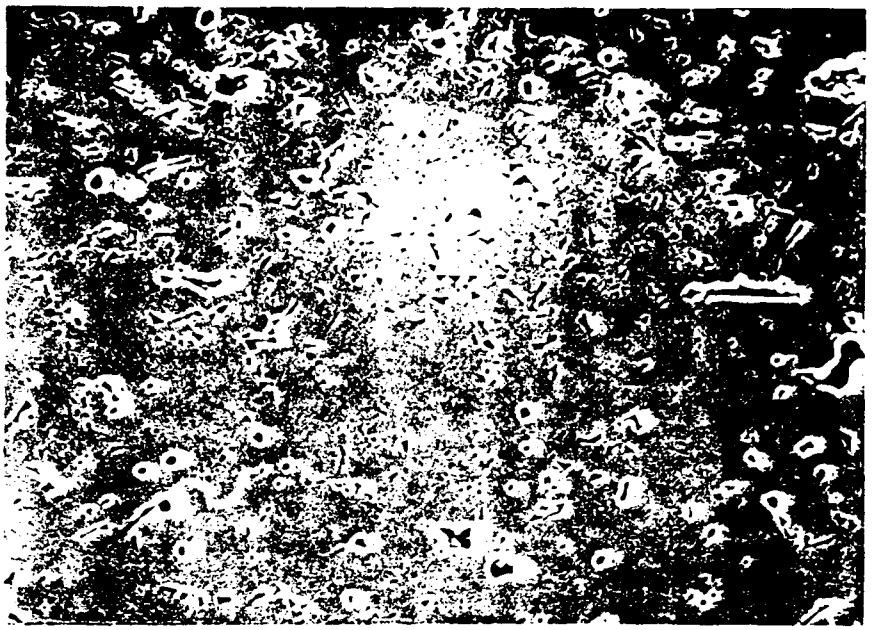

50 μm

50 μm

Figure II-5 SEM micrograph of interface between glass-bonded 95‰ alumina and a) 99.8‰ alumina, and b) sapphire.

Sample A-5 (998P/95/S): The objective of this experiment was to determine whether an increase in bonding temperature, coupled with a polished or a polished and flat surface would lead to a further improvement in the degree of bonding compared to those observed in samples A-4 and A-3.

The *95/S* interface was essentially completely bonded, as illustrated in Figure II-6a.. The sapphire seed had grown into the alumina nearly everywhere, and in most micrographs, it was not possible to deduce the original sapphire/alumina interfacial position unambiguously from the interfacial microstructure. There were also completely bonded sections along the *998P/95* interface, however, there were other sections in which the two pieces were largely unbonded. The average ‰ bonding for the interface was 54‰, however, the standard deviation was also large, ±24‰. An example of the interfacial structure is provided in Figure II-6b.

Summary and Discussion

Several trends are evident from the data. Samples with polished flat surfaces bond more completely than chemically equivalent samples with unpolished surfaces. Consequently, if large pieces are to be bonded using the specific glass-bonded alumina interlayers employed for this study, and the conditions tested, procedures for producing flat polished surfaces must be developed. We are exploring a number of surface preparation methods that could be applied to larger pieces than those examined here. Greater emphasis on characterizing surface flatness will be required. The results also indicate that an increase in bonding temperature is beneficial to producing a higher quality joint. However, it would be desirable to avoid joining at 1700°C. Since the stresses imposed during bonding were minimal, a somewhat higher load should permit the fabrication of better quality bonds at lower bonding temperatures, and allow us to avoid the potentially detrimental changes in the microstructure that can occur at high temperature.

Some aspects of the results were surprising. The 95% alumina used was much more refractory than expected. Wiederhorn *et al.* [8] have examined the creep and fracture of a vitreous bonded alumina (AD-96) from Coors, containing ≈96‰ alumina with the balance glass, and reported the onset of "significant creep activity" at ≈950°C. At 1050°C, creep of AD-96 was rapid. We expected our material would behave similarly. Instead, there appears to be very little creep of the 95% glass-bonded alumina interlayers at 1600°C. Although our applied stress was small, we expected the higher bonding temperature to at least partially offset the stress difference. This was not the case. The results suggest that with improved surface preparation procedures, which should improve the degree of bonding, the 95% alumina will be useful to temperatures several hundred degrees higher than AD-96.

50 μm

50 μm

Figure II-6 SEM micrograph of interface between glass-bonded 95‰ alumina and a) sapphire, and b) 99.5‰ alumina.

III. Joining With Glass Interlayers:

Introduction

For high temperature applications, direct bonding of alumina to alumina has the advantage of providing a joint with the thermal and elastic characteristics of the joined pieces, and of introducing no new chemical constituents that could interact with the alumina and degrade the integrity of the joint. Unfortunately, direct bonding imposes limitations on the joint geometry, requires flat and smooth surfaces, and often a substantial load must be sustained for long periods of time. The results of Section I, and our more general experience in diffusion bonding sapphire to alumina are consistent with these generalizations.

The use of glass-bonded interlayers shows considerable promise as a means of joining alumina to sapphire. There seems little doubt that the conditions used were far from optimum, and that high quality joints could be produced. Measurements of high temperature creep rates, high temperature fracture strength, and of the time dependence of these quantities are necessary to determine whether the bonds will be suitable for extended high temperature use. There are indications in the literature that the creep resistance of such materials can be improved substantially by annealing; a post-joining anneal would, in principle, have the same effect.

Sealing with glasses, although not without its own difficulties, offers some advantages over direct bonding and the use of glass-bonded interlayers. Since oxide glasses generally wet oxide ceramics, a glass will flow at high temperature, and as a result, alternative joint geometries can be considered. Flow also reduces the need to prepare highly polished and mated surfaces. Glass sealing can be relatively rapid, and requires a lower load (if any at all). Finally, the composition of the glass can be modified to produce a range of interfacial compositions and microstructures.

As a result of these considerations, the use of glasses to seal alumina to sapphire was investigated, with a specific focus of producing joints that would be capable of sustained operation at temperatures of up to 1500°C. In independent work, the wetting behavior of six refractory glasses on a high-purity alumina was assessed. The results of this study are included. The ensuing section also describes the result of wetting experiments on sapphire using five of the six glasses, and microstructural and microchemical analyses of the interfacial regions. This is an important first step to identifying glasses that merit further exploration.

Experimental Procedure

Glass Synthesis

Glasses appropriate for a sealing temperature in the range of 1600°C to 1650°C were sought. A range of glass formulations encompassing binary (Al_2O_3-CaO), ternary (Al_2O_3-CaO-SiO_2, Al_2O_3-SiO_2-MgO), and quaternary (Al_2O_3-CaO-SiO_2-ZrO_2) glasses were selected. The specific compositions of the glasses are summarized in Table I.

The glasses were fabricated from the following starting materials: alumina powder (Alcoa CT-3000 SG), MgO powder (Merck), $CaCO_3$ powder (Merck), SiO_2 powder (quartz, Belgian sand), and $ZrSiO_4$ powder (zircon, Quiminsa, Spain, Opazir S.). All powders are nominally 99.9% pure. Calcium carbonate and zircon powders were used as the sources of CaO and ZrO_2, respectively.

TABLE I - Glass Compositions (wt %)

Designation	SiO_2	Al_2O_3	MgO	CaO	ZrO_2
I	--	53.0	--	47.0	--
II	40.0	45.7	--	14.3	--
III	55.0	27.0	18.0	--	--
IV	36.9	44.5	--	11.6	7.0
V	35.0	40.0	--	25.0	--
VI	28.9	36.0	--	28.6	6.5

Two batches of glass of each composition were prepared, using different processing methods. Batch I was prepared by grinding and mixing 2 g of the desired powder mixture in an agate mortar using isopropyl acid. After drying, the powders were isostatically pressed at 200 MPa into a bar of 5 mm diameter. Pellets, weighing 0.3 g, were loaded into Pt capsules, and were fired for 3 h at 1600°C. The samples were then air quenched, and examined visually. The results of the inspection are summarized in Table II.

TABLE II - Glass Characteristics

Designation	Appearance
I	Yellow/brown, transparent
II	Crystallized, glass-ceramic
III	Colorless, transparent
IV	Crystallized, glass-ceramic
V	Colorless, transparent
VI	Colorless, transparent

For Batch II, 100 g of the desired powder mixture was blended in a high speed agitator in an isopropyl alcohol media. Subsequently, the suspensions were dried and the powders were isopressed at 200 MPa into bars of 1.5 cm diameter. The bars, which weighed ≈50 g each, were loaded into a Y-PSZ crucible and fired for 3 h at 1600°C. The Y-PSZ crucibles were used due to the very low solubility of ZrO_2 in the glasses.

Wetting Experiments

Small cubes were cut from pieces of each of the glasses. For wetting experiments with sapphire, randomly oriented high-purity sapphire single-crystal wafers from Meller Optics (Providence, Rhode Island)were used. Since these wafers are highly polished, no additional polishing was required. However, the wafers were preannealed for 2 h at 1200°C to eliminate any organic residues that might have been on the surface. For wetting experiments with alumina, plates (99.5% pure, Coors) were polished, and subsequently preannealed for 4 h at 1200°C in air to remove any residual organics on the surface. The glass cubes were placed onto the substrates. The ensemble was heated in 2 h to 1600°C, held at temperature for 2 h, and then cooled in 2 h to room temperature. The heat treatments were carried out in air. Contact angles were measured at room temperature using a telegoniometer. Samples were inspected visually and using optical microscopy.

Interface Analysis

Samples were cut through the center of the glass sessile drop using a diamond wafering saw. Both cross-sections were polished to a 1 μm finish. One cross section was thermally or chemically etched to reveal the microstructure of the sapphire/sessile drop or alumina/sessile drop interface. This etched sample was also used for EDS analysis. The other as-polished cross section was used for microprobe analysis, and etched subsequently to reveal the microstructure of the traversed region.

Results and Discussion

Contact Angle Measurements: Alumina

The results of room temperature contact angle measurements on alumina, and visual and optical microscopy examination of the samples are summarized in Table III-A. The contact angles were acute for all six glasses tested. Four of the six glasses produced crack-free interfaces.

TABLE III-A Wetting behavior, seal characteristics: alumina

Designation	Contact angle (degrees)	Observations
I	25	Fracture at and near interface
II	23	No cracks evident
III	15	Crack in the glass
IV	19	No cracks evident
V	14	No cracks evident
VI	9	No cracks evident

Of the six glasses examined, glasses I and III did not achieve equilibrium sessile drop shapes. The glass "drop" retained some of the sharp corners and edges present on the initial glass cube. The reported contact angle was measured along the perimeter of these drops, and may not represent a true equilibrium value. It is also possible that the cracking observed in these two samples is related to the relatively thicker glass layer.

Contact Angle Measurements: Sapphire

The observations made in conjunction with contact angle measurements on alumina suggested that Glass I would not be suitable for use with sapphire, and as a result, only Glasses II through VI were tested on sapphire. Visual and optical microscopy examination of the sapphire/glass samples are summarized in Table III-B. The contact angles were acute for all five glasses tested, and similar to those obtained with alumina. Three of the five glasses produced crack-free samples.

TABLE III-B Wetting behavior, seal characteristics: sapphire

Designation	Contact angle (degrees)	Observations
I	--	Not tested
II	26	Cracks in sapphire
III	16	Cracks in sapphire
IV	16	No cracks evident
V	22	No cracks evident
VI	13	No cracks evident

Of the five glasses examined, Glass VI did not achieve an equilibrium sessile drop shape. The drop perimeter morphology suggests that the drop was continuing to expand, possibly because of reaction-driven wetting.

Interface Analysis

Glass I (CaO-Al_2O_3): The equilibrium phase diagram for the CaO-Al_2O_3 system is provided as Figure III-1. When glass of the composition indicated as I is placed in contact with alumina at 1600°C, dissolution of alumina is expected. When the glass composition at the interface reaches the liquidus, $CaAl_2O_4$ precipitates can begin to form. However, neither the glass nor the precipitates are in equilibrium with alumina. If continued dissolution of alumina is possible, the glass will ultimately be replaced by calcium aluminates of progressively higher alumina content. Kinetics permitting, one would ultimately expect equilibrium between alumina and $CaAl_{12}O_{19}$.

Glass I/Alumina: At low magnification, Figure III-2, the attack of the glass on the substrate is evident; the alumina/glass interface was originally flat. Severe degradation of the surface may be undesirable. It is also apparent that an equilibrium sessile drop shape did not develop. Consequently, if this glass were to be used, a higher bonding temperature might be necessary, and this would change the microstructure evolution of the interfacial zone. However, the high viscosity at 1600°C suggested by incomplete drop equilibration, is desirable from a deformation standpoint. As was indicated in Table III-B, the sample failed at and near the interface. The failure of the drop to equilibrate, which leads to a very thick glass layer, may contribute to this (mechanical) failure.

As shown in Figure III-3, the interface contains regions of lighter and darker contrast, which usually indicate compositional differences. This contrast variation is most noticeable nearer the center of the drop. EDS analysis indicates that both regions contain predominantly aluminum and calcium as cations. Analysis of the darker regions suggests a composition of 45.9 wt % (55.7 at %) Al and 54.1 wt % (44.3 at %) Ca. The composition of the lighter regions is only slightly different - 45.2 wt % (55.0 at %) Al and 54.8 wt % (45.0 at %) Ca. EDS detects only the cations, not oxygen. In terms of cations only, as-prepared Glass I would be analyzed as 55.4 at % Al and 44.6 at % Ca. The aluminum and calcium contents of the two regions differ only slightly from, and bracket these values. The compositions of the two regions coincide most closely with that of $Ca_{12}Al_{14}O_{33}$ (46.2 at % Ca, 53.8 at % Al). High temperature phase diagrams of the CaO-Al_2O_3 do not indicate two phases adjacent to $Ca_{12}Al_{14}O_{33}$ that have compositions similar to those of the two observed regions.

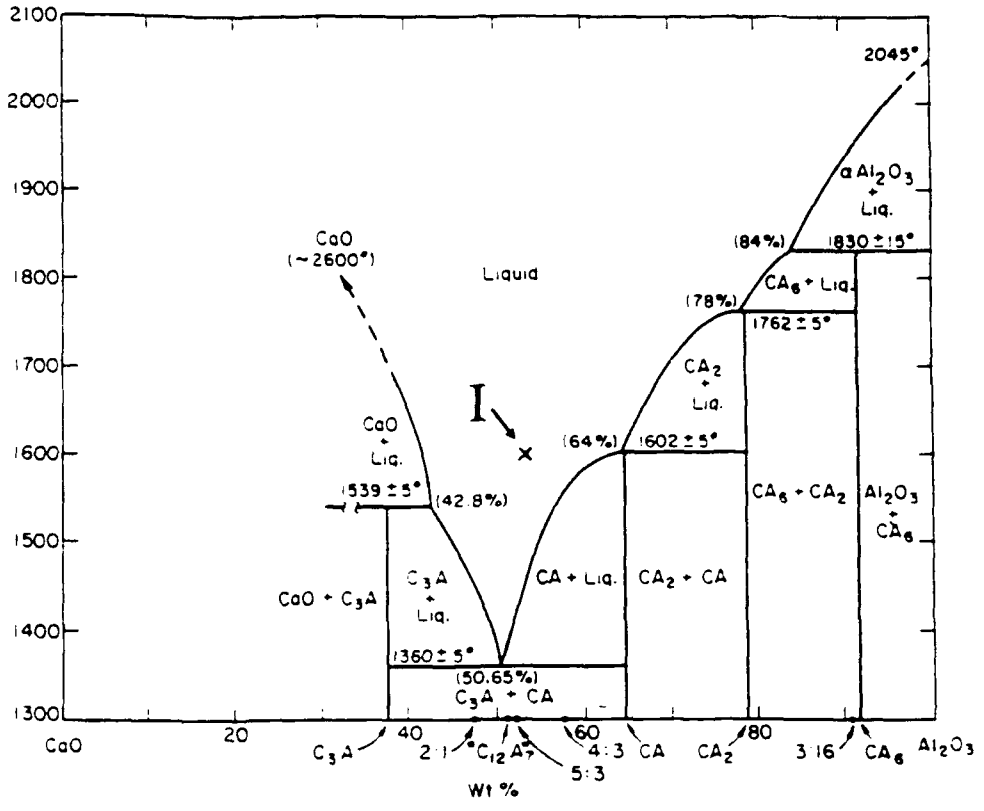

Figure III-1 The phase diagram of the Al_2O_3-CaO system as presented in PHASE DIAGRAMS FOR CERAMISTS.

Figure III-2 Low magnification (9.4X) SEM micrograph of the cross section of a "drop" of Glass I on alumina.

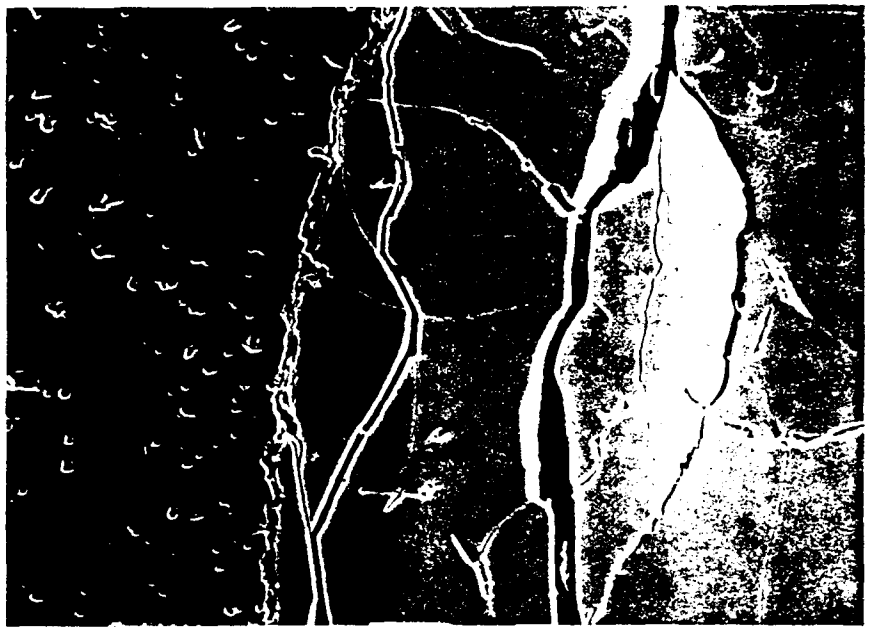

Figure III-3 Higher magnification (250X) SEM micrograph of the alumina/Glass I interface. Alumina is on the left; Glass I is on the right.

The EDS results were puzzling, and several possible explanations were considered. If the EDS analyses are correct, the differences in contrast could reflect incomplete homogenization of the glass during fabrication and sealing, rather than the presence of two phases. Alternatively, the phases that form may be metastable phases that do not appear on the equilibrium diagram. However, it appeared more likely that the EDS analysis was not quantitatively correct. Microstructural analysis of the sample suggests substantial dissolution of alumina by the glass, whereas the composition obtained by EDS analysis implies that relatively little dissolution occurred during the 2 h anneal at 1600°C.

Microprobe line and raster scans were conducted to determine the composition of the glass and the interfacial region more accurately. Results of a representative line scan and a micrograph of the scanned region are shown in Figure III-4. There is evidence for the formation of a reaction layer at the alumina/Glass I interface. This layer, which is ~10 µm thick is not apparent in lower magnification micrographs. Since the highest alumina content is expected right at the alumina/Glass I interface, this darker region may represent one of the higher alumina content crystalline phases that appear in the phase diagram. More generally, the microprobe results are consistent with the findings of EDS in that there is little spatial variation in the composition of the glass. The two "phases" have essentially the same composition. However, a major difference exists between the compositions indicated by the EDS and microprobe analyses. Microprobe analysis indicates an average composition of ≈66 wt % Al_2O_3, ≈34 wt % CaO. This is consistent with considerable dissolution of alumina.

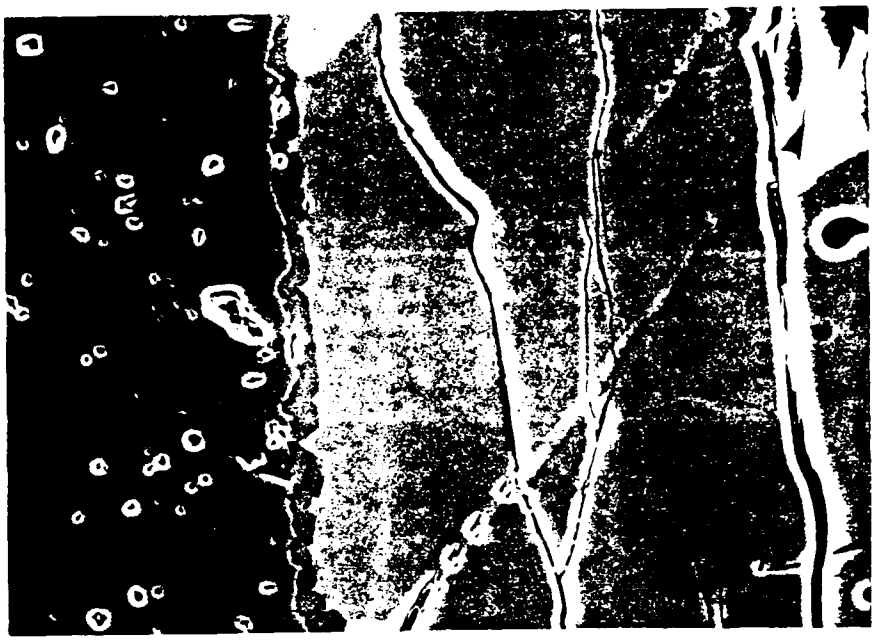

50 µm

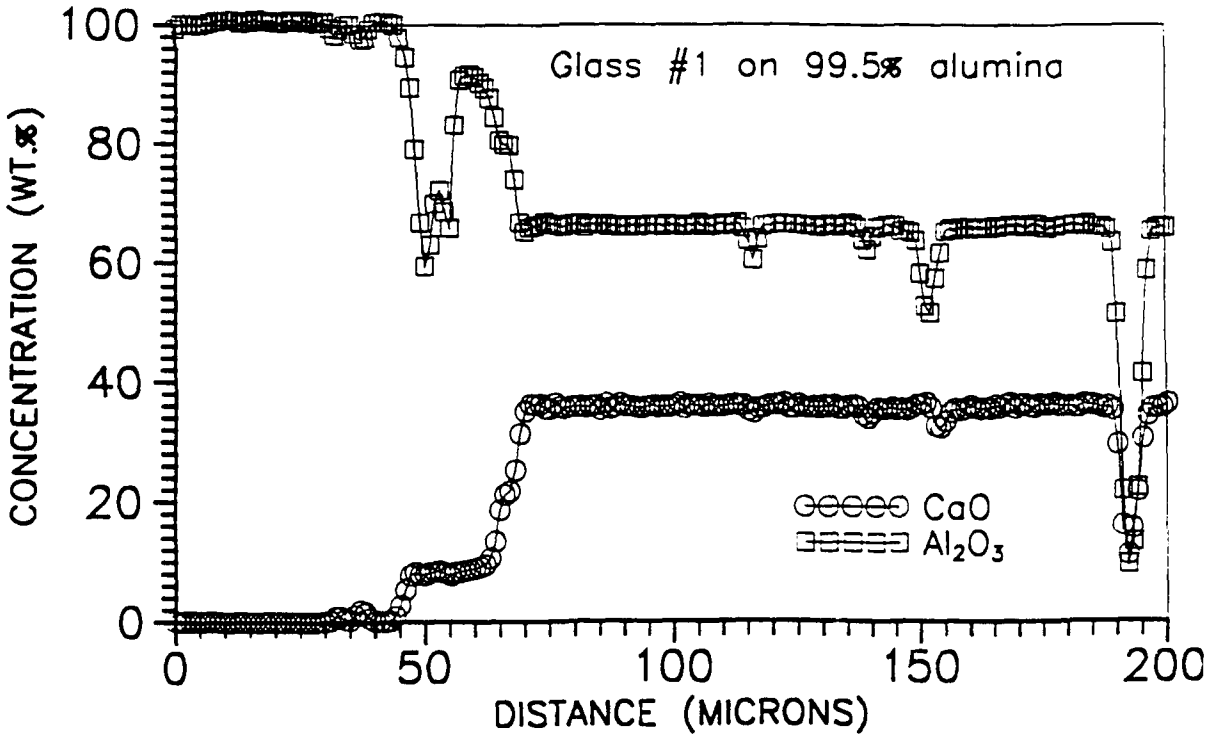

Figure III-4 SEM micrograph (501X) and microprobe line scan of the alumina/Glass I interface.

If this compositional analysis of the glass is quantitatively correct, the phase diagram provides an explanation for the observed structure. During dissolution of alumina, the glass will ultimately become supersaturated with respect to $CaAl_2O_4$ (CA). Continued dissolution of alumina will cause continued precipitation of CA. Note that the equilibrium composition of the glass at 1600°C is slightly less than 64 wt % Al_2O_3, while that of CA is 64.5 wt % Al_2O_3. We suggest that dissolution has progressed to the point where a liquid and CA coexist at 1600°C. During cooling, CA persists. Since the drop perimeter moves outward during annealing, the glass at the drop perimeter has not been in contact with alumina for as long as the interior. Plausibly, the perimeter region does not have as high an alumina content as the interior, and as a result, does not develop the two-phase structure. X-ray diffraction of the glass is being used to identify any crystalline phases that have formed during cooling.

Glass II (CaO-Al_2O_3-SiO_2): The equilibrium phase diagram for the CaO-Al_2O_3-SiO_2 system is provided as Figure III-5, and the composition of Glass II is indicated by the point II. At 1600°C, the glass composition lies within a two-phase field involving equilibrium between liquid and corundum. The alumina content of the glass exceeds that of the liquidus composition. As a result, one expects precipitation of alumina throughout the glass, and alumina depletion of the glass (in comparison to its initial alumina content). No dissolution of alumina should occur. Since neither silica nor calcia are soluble in alumina to any significant extent, one also would expect that the glass would be in equilibrium with essentially pure alumina. As a result, quenching should produce a microstructure of predominantly glass, with 5-10 wt % alumina crystallites. If the glass is cooled sufficiently slowly, the equilibrium room temperature microstructure of the bulk Glass II would consist of primarily anorthite and mullite, with potentially a very small amount of silica. The actual microstructure will vary between these extremes and reflect the thermal history.

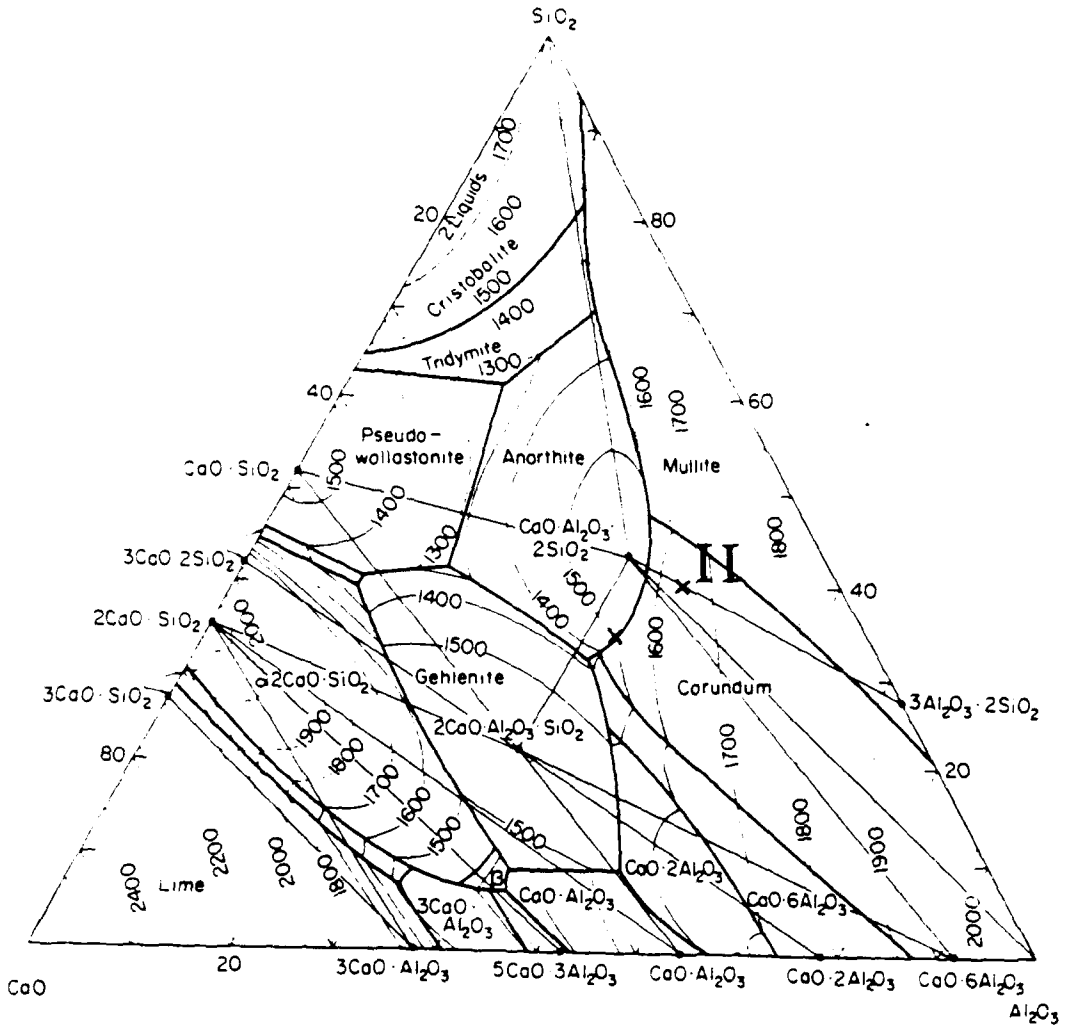

Figure III-5 Phase diagram of CaO-Al_2O_3-SiO_2 system as presented in PHASE DIAGRAMS FOR CERAMISTS.

Glass II/Alumina: Low and higher magnification SEM micrographs of the alumina/Glass II interface are provided in Figures III-6a and III-6b, respectively. The formation of platelike precipitates throughout the glass is indicated. Presuming this phase to be alumina, its volume fraction is qualitatively consistent with expectations. The glass contains numerous bubbles, which appear to act as heterogeneous nucleation sites for the crystalline phase.

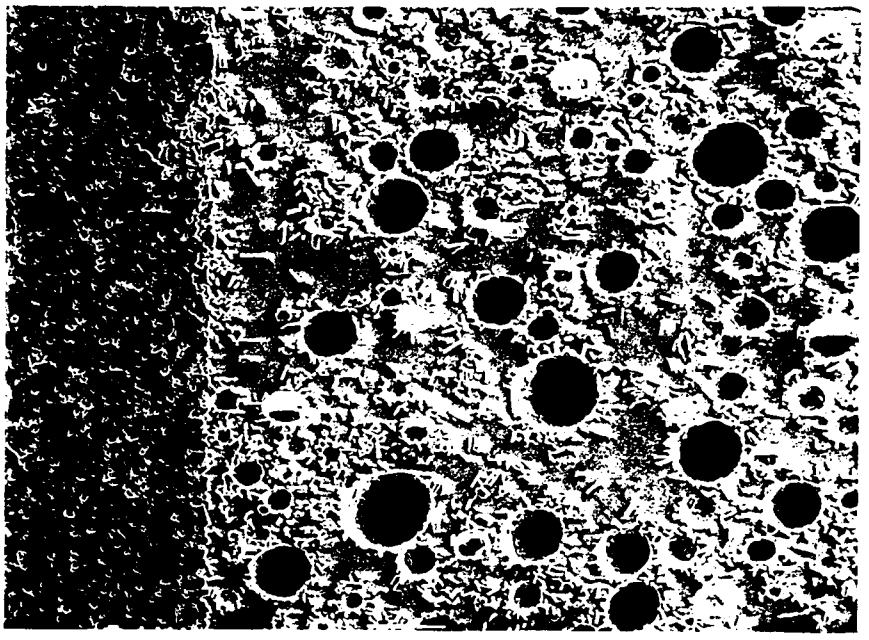

250 µm

75 µm

Figure III-6 a) Low magnification (99X) and b) higher magnification (310X) SEM micrographs of alumina/Glass II interface.

X-ray mapping and microprobe line scans were used to provide chemical information on the platelike crystallites that formed either during annealing, or during cooling to room temperature. Figures III-7a-7d provide an SEM micrograph of the interface (7a), and x-ray maps for Al (7b), Ca (7c), and Si (7d). The results suggest that the particles are aluminum rich, as expected from the phase diagram. The results of a focussed beam microprobe scan across the interface and the microstructure of the scanned region are shown in Figure III-8. As the platelike particles are probed, there is a corresponding increase in the alumina concentration to ≈100%. This analysis is consistent with the x-ray mapping data, and indicates that the angular platelike precipitated phase is indeed alumina. The composition of the glass is indicated to be 50 wt % SiO_2, 32 wt % Al_2O_3, and 18 wt % CaO. This alumina content is lower than expected, and places the composition of the residual glass in the anorthite primary crystalline phase field. However, we note that this composition does lie on the extended tie line between the bulk composition of Glass II indicated in Table I and alumina.

50 μm

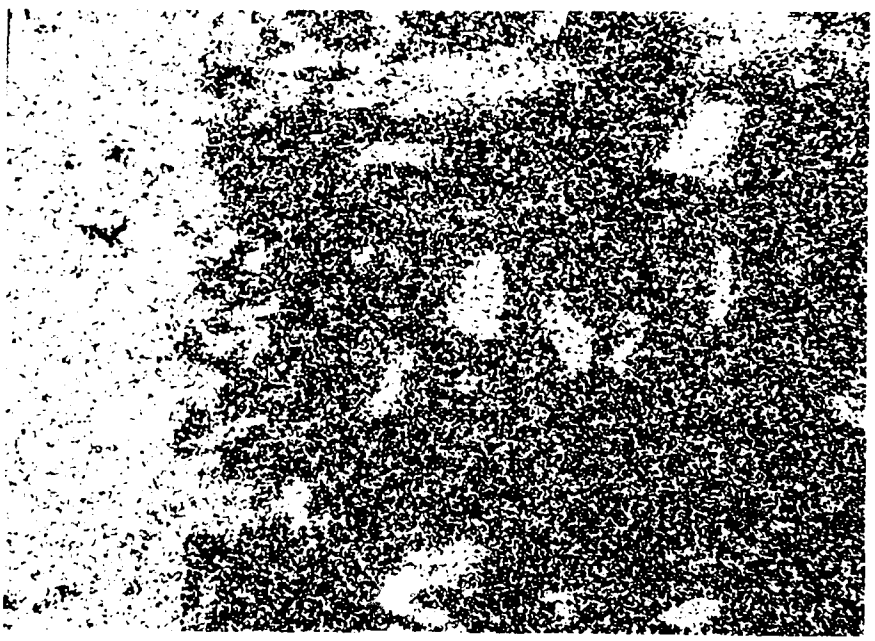

50 μm

Figure III-7 a) SEM micrograph (490X) of alumina/Glass II interface and b) accompanying x-ray map for aluminum.

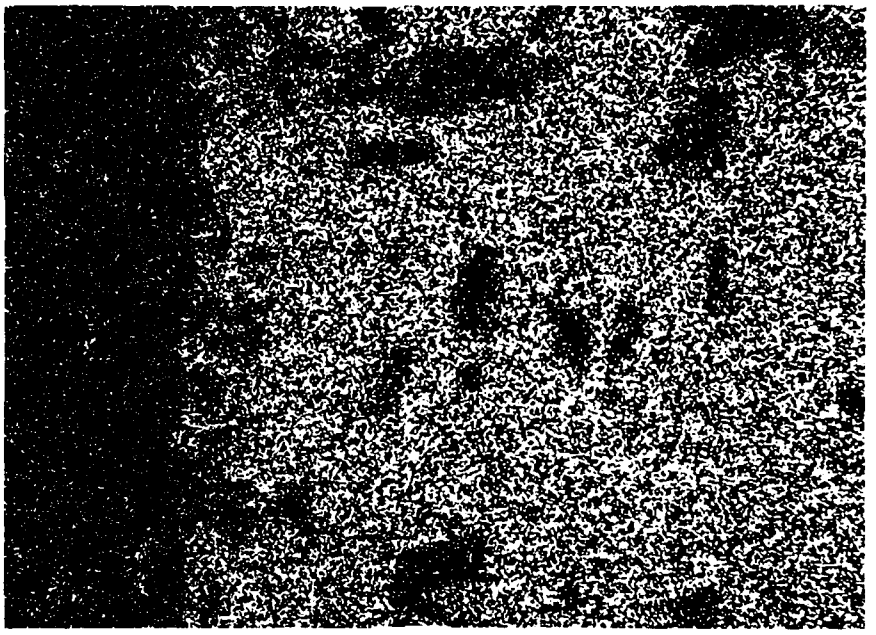

50 μm

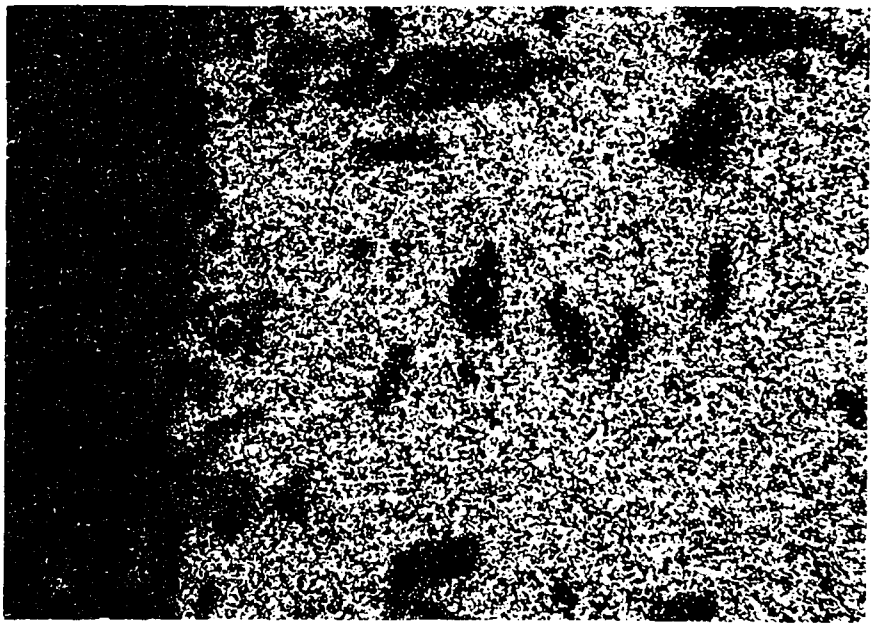

50 μm

Figure III-7 (cont.) X-ray maps of c) calcium and d) silicon at alumina/Glass II interface.

50 μm

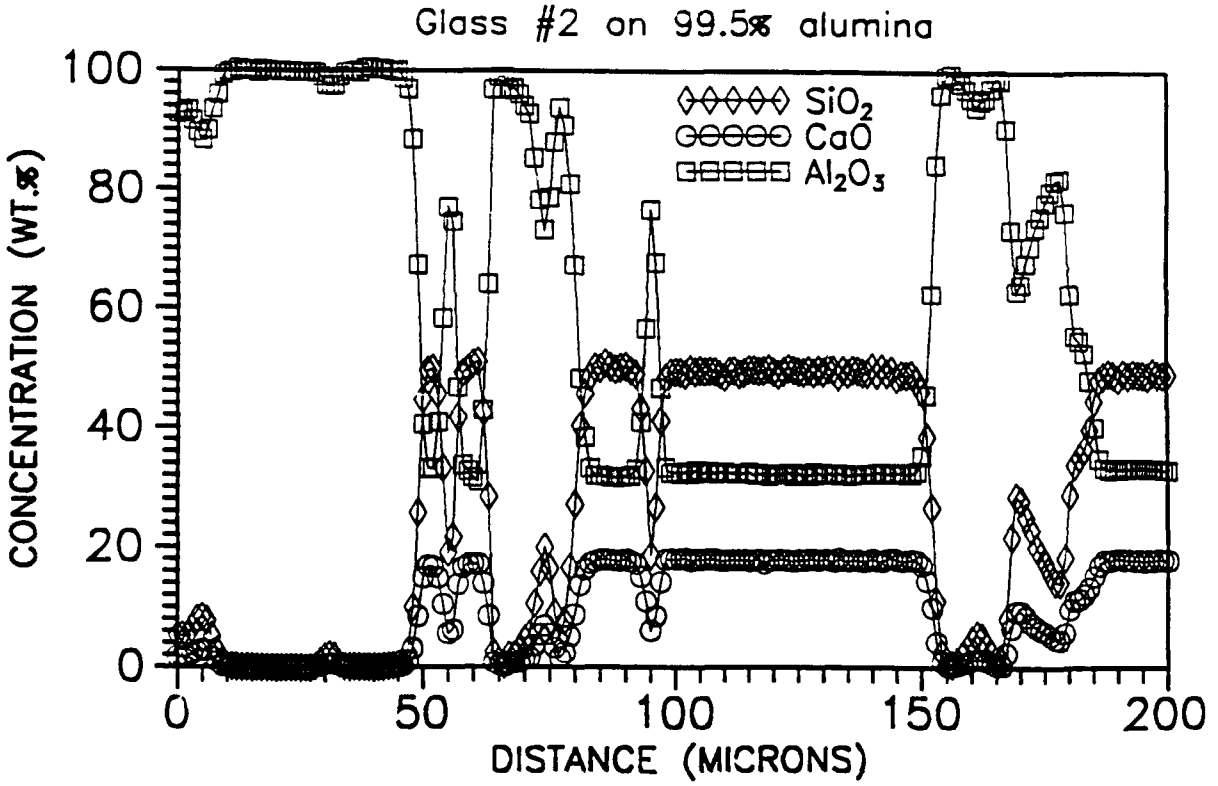

Figure III-8 SEM micrograph (501X) of alumina/Glass II interface, and results of microprobe scan.

The cross sections also indicate the presence of a smaller volume fraction of a second less angular precipitate. The x-ray maps fail to provide a clear indication of the composition of such particles, and the microprobe trace failed to traverse such a particle. SEM/EDS spot analyses suggest a precipitate cation composition of 25.2 wt % (28.6 at %) Al, 43.3 wt % (47.3 at %) Si, and 31.5 wt % (24.1 at %) Ca. However, the accuracy of these results is questionable. For example, EDS analysis of bulk Glass II indicated 29.7 at % Al, 45.5 at % Si, and 24.8 at % Ca. These values differ substantially from the true bulk glass composition. These results, and those reported for Glass I, indicate that EDS analyses of such glasses provide an indication of the constituents, but do not measure the composition accurately. We speculate that this second precipitate may be anorthite.

From a chemical standpoint, this glass formulation is attractive because the glass readily equilibrates with the alumina. From a high temperature application standpoint, the glass has potential limitations. If the glass equilibrates with alumina at 1600°C, and the glass composition remains fixed during cooling, the first liquid should also form at ≈1600°C during heating. If instead the liquid composition adjusts during cooling via the precipitation of additional alumina, and then undergoes no further chemical change, the equilibrium phase diagram suggests that a liquid could form at ≈1520°C. Thus, ensembles joined using this glass could be unsuitable for applications at 1500°C. If the overall glass composition lies slightly to the silica side of the anorthite-mullite tie line, and therefore within the anorthite-mullite-silica tie triangle, a liquid could form at a temperature as low as 1345°C. In this case, the use temperature of a joined assembly would be reduced further.

Glass II/Sapphire: As was the case in Glass II/alumina samples, platelike precipitates formed throughout the glass (Figure III-9). The glass again contains bubbles, which appear to act as preferential nucleation sites for these particles. In general, the microstructure within the glass is quite similar to that seen in Glass II/alumina samples. The matrix surrounding the platelike particles differs slightly in appearance from that in Glass II/alumina samples, however, this appears to reflect an effect of increased etching time, rather than a difference in chemistry or phase composition.

Perhaps the most important difference between the glass/alumina and glass/sapphire samples was the presence of cracks in the latter. We note that the sapphire used for the present experiments was of random orientation, and the thermal expansion coefficient of sapphire is anisotropic. This cracking may reflect an unfortunate combination of sapphire orientation and glass thermal expansion, rather than a fundamentally poor match between the glass and alumina.

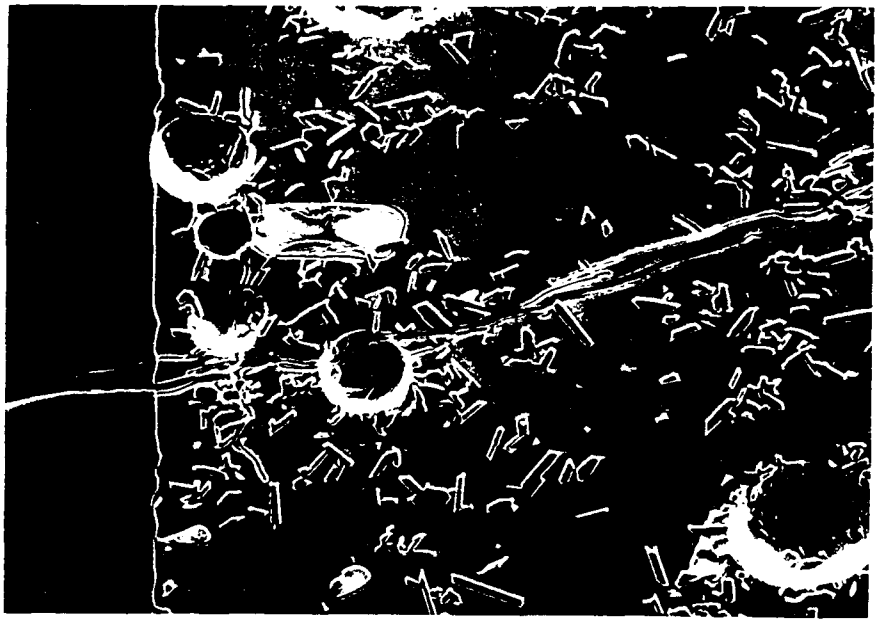

Figure III-9 SEM micrograph (500X) of sapphire/Glass II interface, showing platelike particles and cracking at the interface.

Glass III (Al_2O_3-SiO_2-MgO): The equilibrium phase diagram for the Al_2O_3-SiO_2-MgO system is provided as Figure III-10, and the composition of Glass III is indicated by the point III. The glass is not in equilibrium with alumina, and substantial dissolution of alumina should occur. The extended tie line between alumina and the composition III indicates that the glass equilibrates with alumina when it achieves a composition of ≈42 wt % silica, ≈44 wt % alumina, and ≈14 wt % calcia. At lower temperatures, a material with the composition of this equilibrated glass will lie in the three-phase tie triangle, and thus at equilibrium, one expects a three-phase mixture of primarily cordierite ($2MgO{\cdot}2Al_2O_3{\cdot}5SiO_2$), with lesser amounts of sapphirine ($4MgO{\cdot}5Al_2O_3{\cdot}2SiO_2$) and mullite ($3Al_2O_3{\cdot}2SiO_2$).

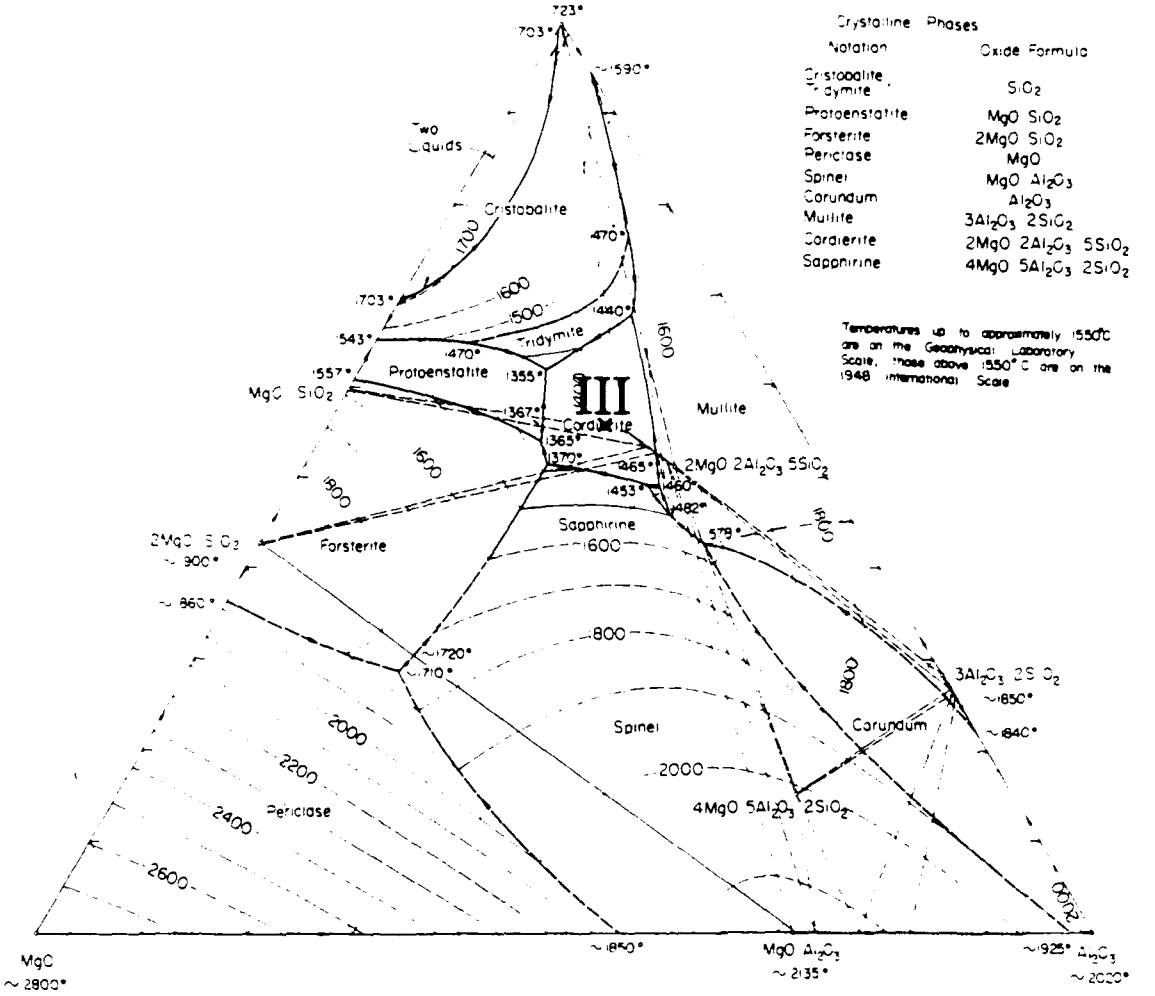

Figure III-10 Phase diagram of Al_2O_3-SiO_2-MgO system as presented in PHASE DIAGRAMS FOR CERAMISTS.

Glass III/alumina: A typical SEM micrograph of the alumina/Glass III interface is provided in Figure III-11. Three morphologically distinct phases are indicated. There is a 40-60 μm thick layer that "coats" the interface. Farther from the interface, platelike particles and a feathery dendritic particle are found. A second micrograph of the interface, and accompanying x-ray maps for Al, Mg, and Si provide an indication of the chemistry of these particles, Figure III-12. The 40-60 μm thick interfacial layer contains Al and Mg as the primary cations. This suggests the layer is spinel. The platelike particles are Al-rich. The signals for Mg and Si appear to be at the background level, suggesting the particles are alumina. The feathery dendritic particles contain all three cations, and have a composition that is similar to that of the residual glass. Plausibly, this phase corresponds to cordierite.

Figure III-11 SEM micrograph (250X) of alumina/Glass III interface. Alumina is on the left; Glass III is on the right.

50 μm

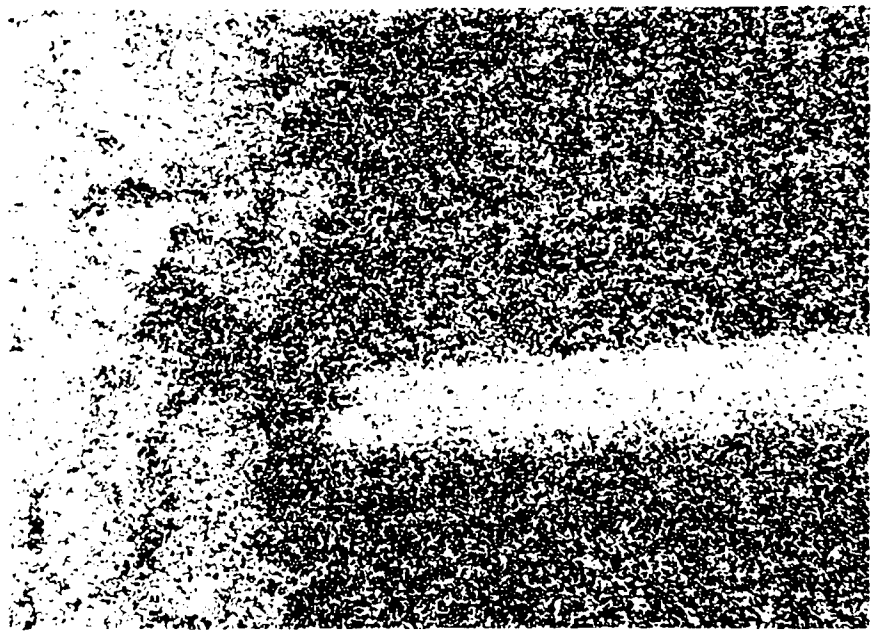

50 μm

Figure III-12 a) SEM micrograph (500X) of alumina/Glass III interface and b) accompanying x-ray map for aluminum.

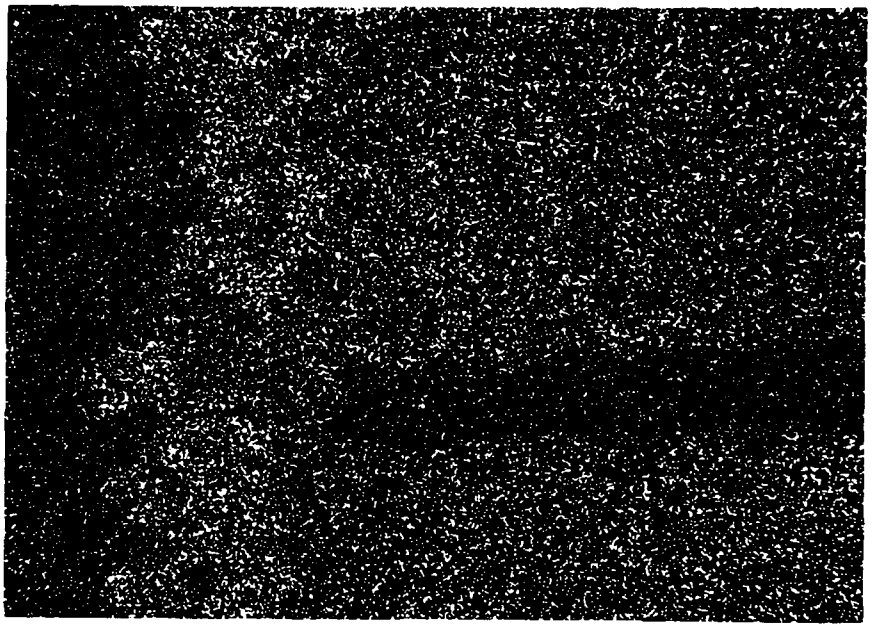

50 µm

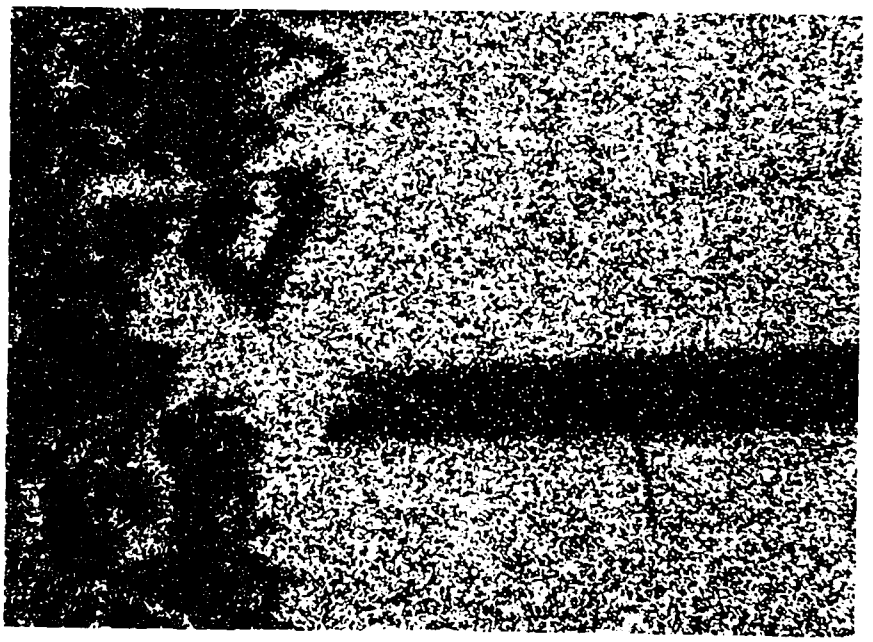

50 µm

Figure III-12 (cont.) X-ray maps of c) magnesium and d) silicon at alumina/Glass III interface.

Microprobe line scans were used to better define the compositions of the phases in the glass. The results of a focussed beam line scan and the microstructure corresponding to the scan are shown in Figure III-13. Some penetration of the glass into the alumina is indicated by both the micrographs and the probe data. There are pockets of glass within the probed volume that lead to sudden changes in the composition, notably, a precipitous drop in the alumina content, and rapid increases in the magnesia and silica content. The regions are sufficiently small in comparison to the probed volume that a constant composition zone is not apparent in the scan. In the transition from the alumina to the glass, we see a region in which Al_2O_3 (≈77 wt %) and MgO (≈23 wt %) are the primary constituents. These values approach those for stoichiometric spinel, ≈72 wt % Al_2O_3 and ≈28 wt % MgO. At 1600°C, the spinel phase field extends from ≈70 to ≈82 wt % Al_2O_3. The residual glass has a composition that is spatially variable, but falls in the range of 12-19 wt % MgO, 28-32 wt % Al_2O_3, and 50-58 wt % SiO_2. This compositional range spans both the cordierite and mullite primary crystallization fields, and includes the initial composition of the glass. In the final ≈70 μm of the trace the beam is traversing one of the feathery particles, and as a result, the signals for alumina, silica, and magnesia vary seemingly erratically. The particles do contain alumina, magnesia, and silica, and even taking into account the uncertainty in the composition values, cordierite appears to be the most logical assignment for these features. The scan did not traverse any platelike particles. As a result, confirmation of the x-ray mapping results is still required.[4]

There are several puzzling aspects to the microstructure that has evolved. There is evidence for penetration of the glass into the alumina, and there does appear to be substantial dissolution of alumina by the glass. It is possible that the degree of dissolution is sufficient to saturate the glass with alumina at 1600°C. However, neither partial nor equilibrium amounts of dissolution provide a glass composition, which upon cooling, should produce the phases that are present. During cooling, the alumina-saturated glass would first precipitate alumina, then spinel and mullite, next sapphirine and mullite, and finally sapphirine, cordierite and mullite during solidification of the eutectic liquid. The alumina should be resorbed, and the final microstructure should consist of a mixture of sapphirine, cordierite and mullite. If the glass is not saturated with alumina, alumina should not appear at all during cooling. If the phase identification is correct, the crystalline phases that are present cannot co-exist at equilibrium; they do not define a compatibility triangle in the equilibrium phase diagram.

Of the glasses examined, Glass III was one of the two that did not achieve an equilibrium sessile drop configuration at 1600°C. As was the case with Glass I, cracks formed in the sample. This cracking may be the consequence of the glass layer thickness, or alternatively, may suggest that thermal expansion mismatch stresses are severe. While the first cause of cracking can be remedied, the second cannot. Since several other glasses did not develop cracks, Glass III is not thought to be a prime candidate for applications in which the temperature is high and thermal cycling is frequent.

---

[4] Unfortunately, when using the probe, coated polished specimens must be used. One can define the general region within which the scan will occur, but one cannot assure that specific microstructural features will be traversed. The microstructure in the scanned region is determined by burning a trace into the mounting resin, and etching the sample after microprobe analysis.

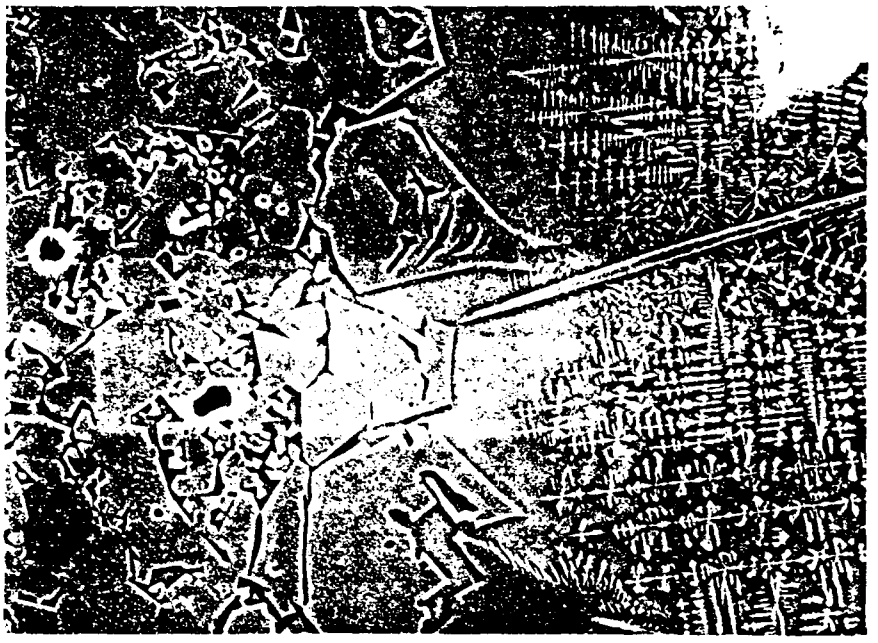

50 µm

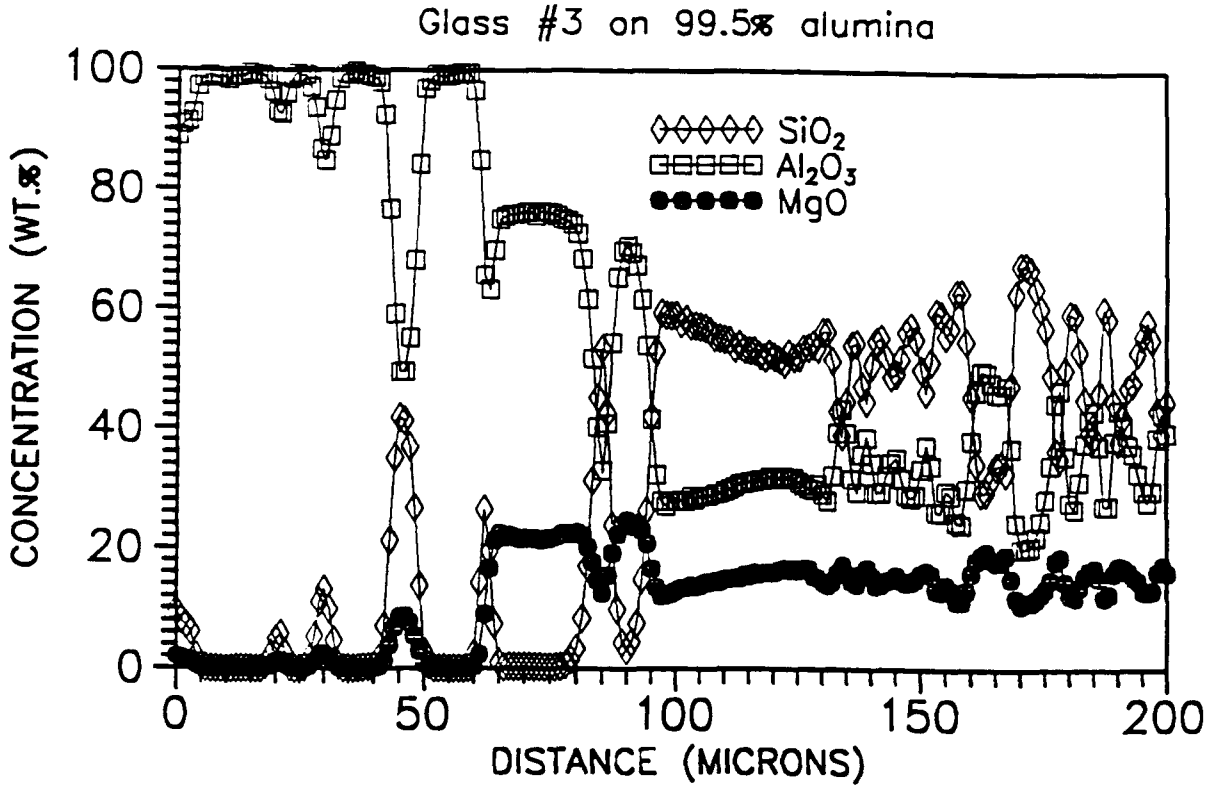

Figure III-13 SEM micrograph (499X) of alumina/Glass III interface, and results of microprobe scan.

Glass III/Sapphire: There was considerable dissolution of sapphire by the glass, with the most pronounced dissolution occurring at the drop center. The spinel layer found at the glass/alumina interface is not evident. Instead, there is evidence of facetting of the sapphire along the interface. For glass/alumina samples, crystalline phases were found throughout the glass. In the present case, there were relatively few instances of crystalline particles within the glass. Possibly, the incorporation of the glassy phase within the alumina during dissolution adds components to the glass that facilitate nucleation of the crystalline particles; the thermal history of the glass/alumina and glass/sapphire samples was identical. Figure III-14 illustrates the facetting, the absence of the spinel layer, and one of the few crystalline particles found in this sample. As was the case with alumina, cracks developed in the sample, and thus, this glass does not appear to be a primary candidate for high temperature applications involving extensive thermal cycling.

Figure III-14 SEM micrograph (500X) of interface between sapphire and Glass III.

Glass IV (CaO-Al_2O_3-SiO_2-ZrO_2): Glass IV is a quaternary glass. The addition of zirconia is expected to increase the viscosity relative to that of a ternary glass with the same calcia to alumina to silica ratio, and thus improve its high temperature capabilities. The interaction of a glass from such a quaternary system with alumina is complex. The microstructure that evolves during cooling will depend upon the extent of reaction, and will be affected by the precipitation kinetics. In general, one can anticipate that as many as four phases can coexist at equilibrium in a quaternary system. The composition of Glass IV is alumina-rich in comparison to the liquidus composition of a glass with the given calcia to alumina to silica ratio used. At 1600°C, alumina should precipitate from the glass, and alumina and a glass of correspondingly lower alumina content are predicted to coexist at 1600°C. There should be no dissolution of alumina by the glass. Precipitation of zirconia is expected during cooling.

Glass IV/alumina: Since the glass is supersaturated with respect to alumina, there should be no attack of the substrate. Low magnification micrographs of the interface confirm this hypothesis. SEM micrographs of the alumina/glass interfacial region indicate that two morphologically distinct phases are present, Figure III-15. The first is a platelike particle, the second has a feathery/dendritic appearance. X-ray maps of the sample, shown in Figure III-16 with the corresponding microstructure, show that the platelike particles contain predominantly aluminum as a cation. The feathery particles do not contain readily detectable amounts of alumina, silica, or calcia, and thus are identified as zirconia. Microprobe scans of the interface support this phase identification, Figure III-17. The microprobe results also indicate that the residual uncrystallized glass has a composition of ≈49 wt % SiO_2, ≈32 wt % Al_2O_3, ≈16 wt % CaO, and the balance (≈3 wt %) ZrO_2.

The development of an equilibrium sessile drop configuration at 1600°C, the absence of possibly harmful corrosion of alumina, and the absence of any cracks in either the glass or the substrate make this glass attractive for high temperature applications. As with most of the glasses that have been studied, the strength-temperature characteristics of a joined assembly will need to be tested.

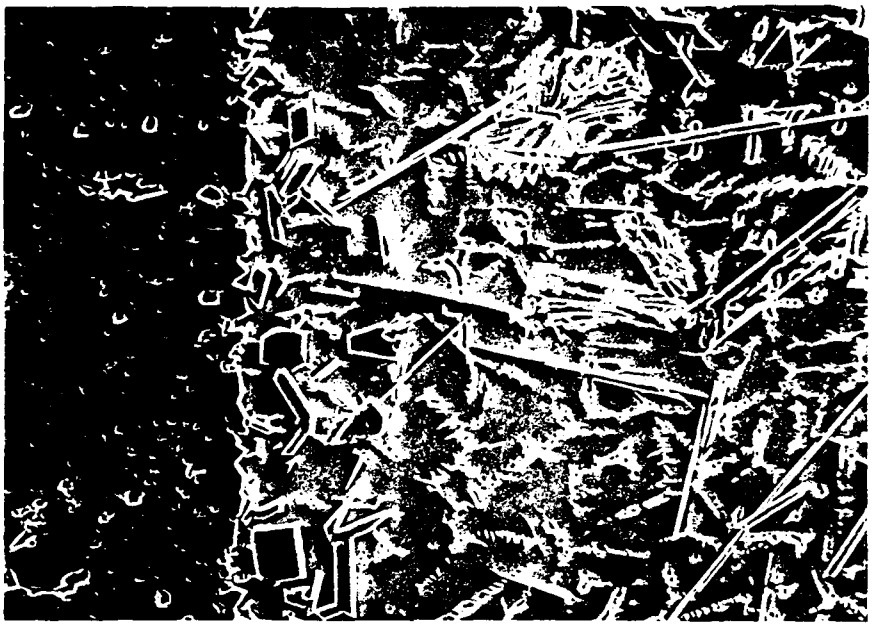

100 μm

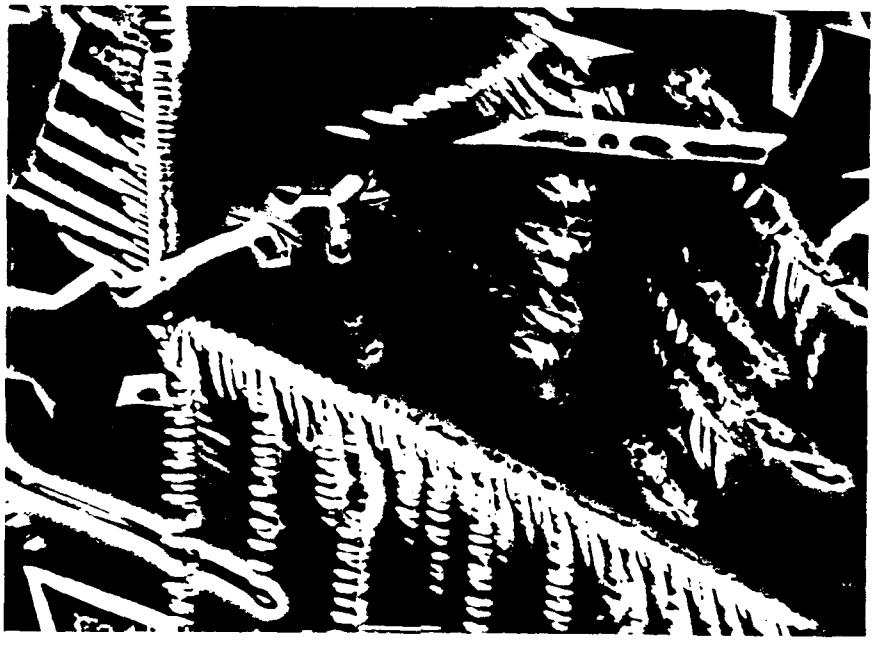

25 μm

Figure III-15 a) Lower magnification (250X) SEM micrograph of alumina/Glass IV interfacial region and b) higher magnification (1000X) SEM micrographs of precipitates in Glass IV.

50 μm

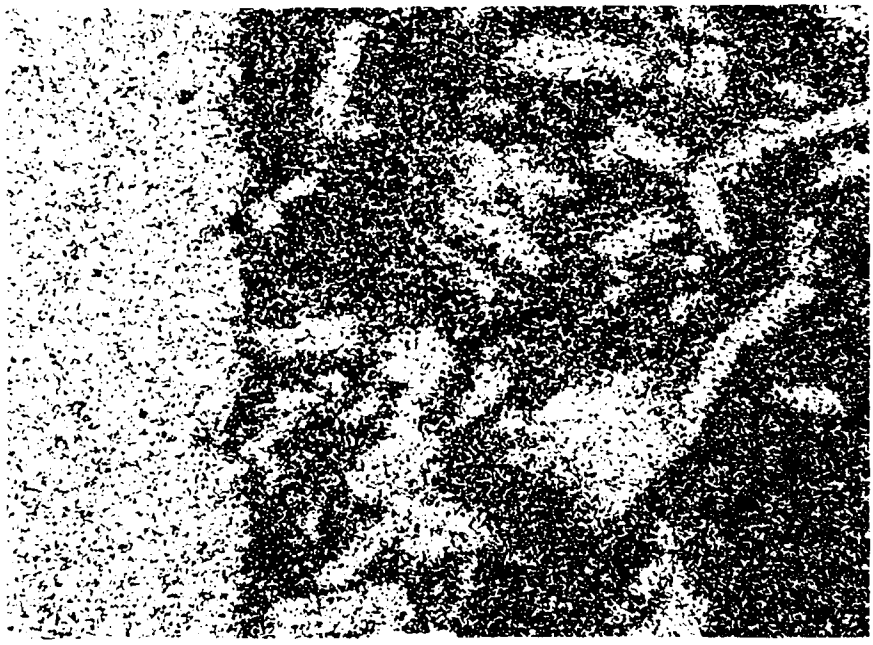

50 μm

Figure III-16 a) SEM micrograph (500X) of alumina/Glass IV interface and b) accompanying x-ray map for aluminum.

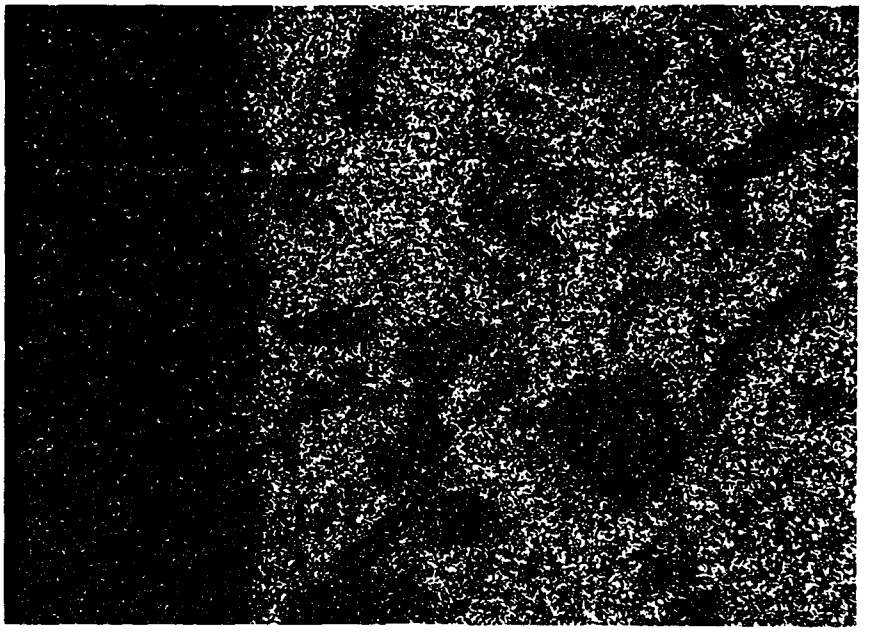

50 μm

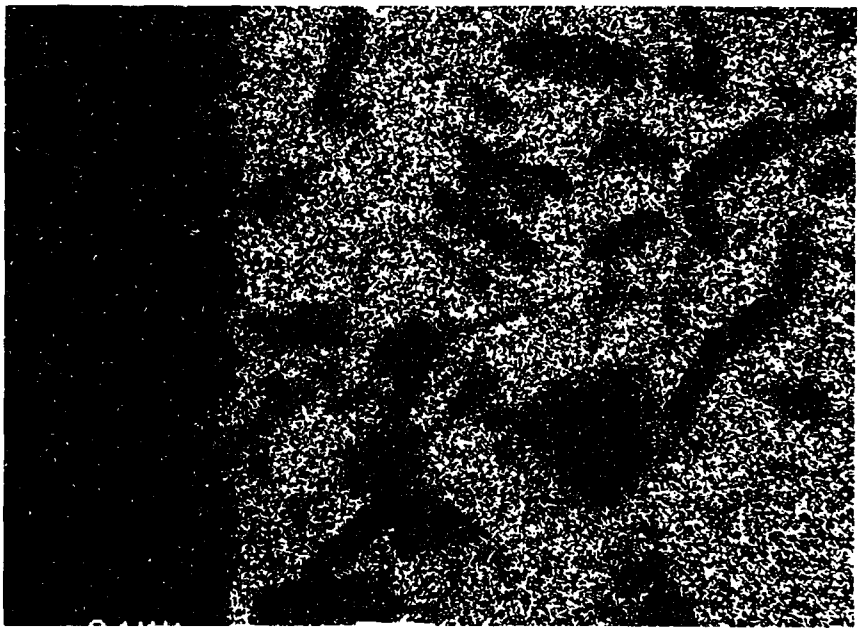

50 μm

Figure III-16 (cont.) X-ray maps of c) calcium and d) silicon at alumina/Glass IV interface.

50 μm

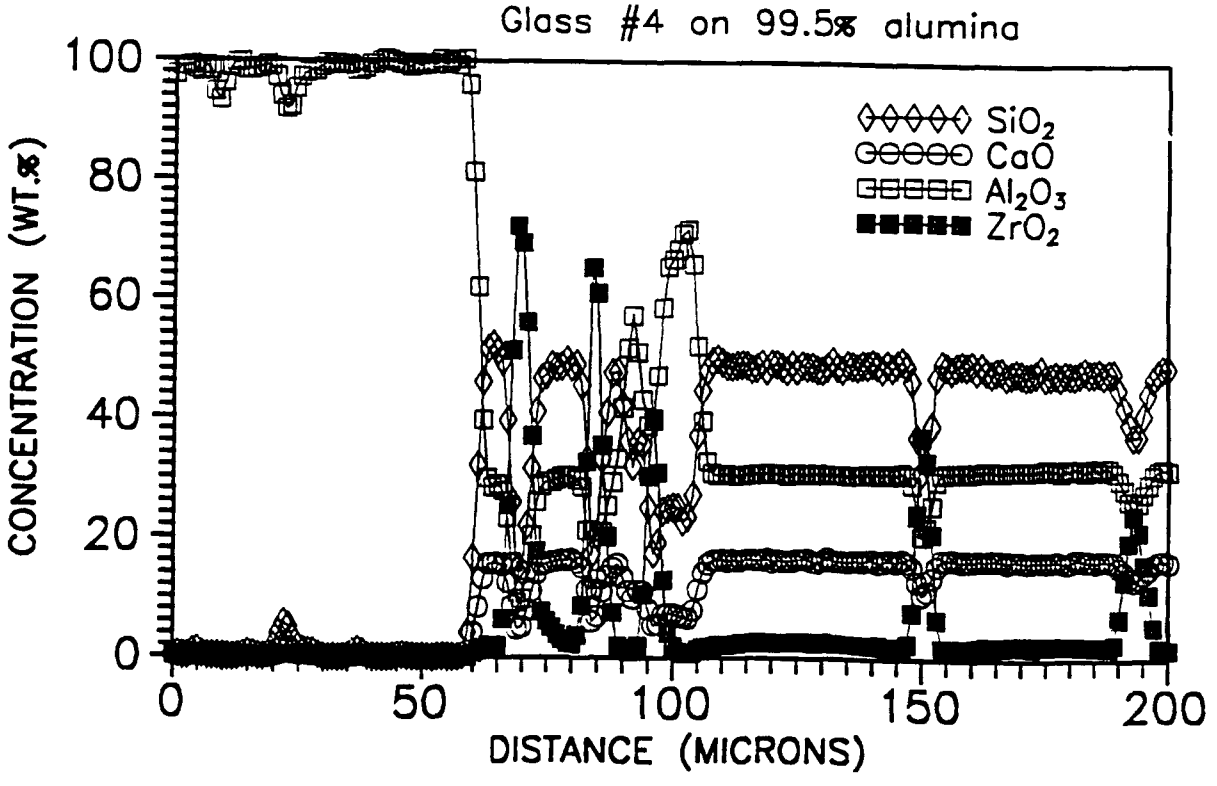

Figure III-17 SEM micrograph (500X) of alumina/Glass IV interface, and results of microprobe scan.

Glass IV/Sapphire: There were no significant differences between the glass/sapphire and glass alumina samples. There is some roughening of the sapphire, however, there does not appear to be any substantial dissolution of sapphire. The roughening may simply be reflective of surface energy anisotropy, and the onset of facetting. Both a platelike particle, presumably alumina, and a feathery/dendritic particle were found distributed throughout the glass. A typical microstructure is shown in Figure III-18.

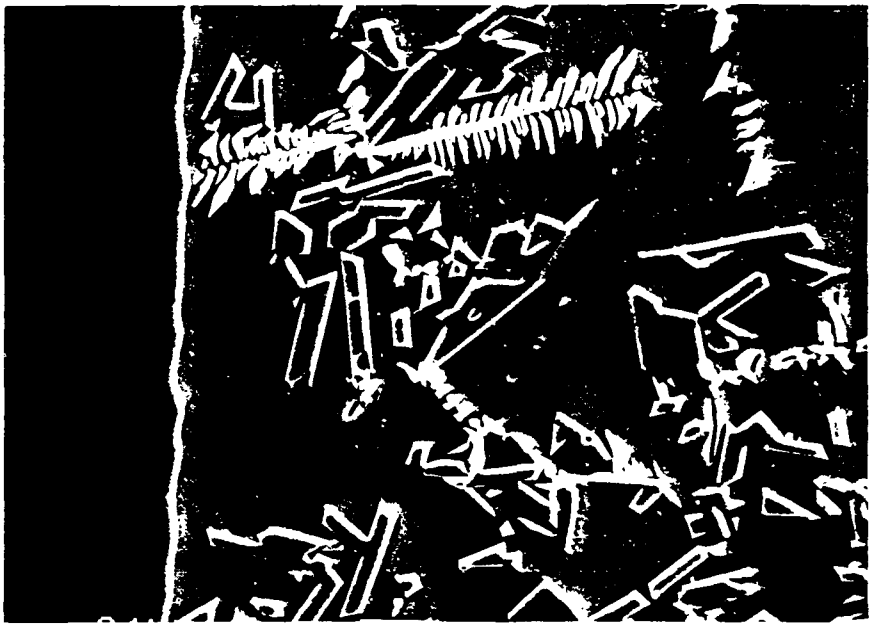

Figure III-18 a) SEM micrograph (500X) of sapphire/Glass IV interface.

Glass V (CaO-Al_2O_3-SiO_2): Glass V is from the same ternary system as Glass II, however, the composition lies within the anorthite primary crystallization field, and close to the boundary of the anorthite field with the corundum field. Dissolution of alumina at 1600°C is expected. During cooling from 1600°C, alumina should precipitate, until the boundary line between the corundum and anorthite fields is encountered. During subsequent cooling, alumina and anorthite should precipitate. Precipitated alumina should then be resorbed, and coprecipitation of anorthite ($CaO{\cdot}Al_2O_3{\cdot}2SiO_2$) and CA_6 ($CaO{\cdot}6Al_2O_3$) is expected. If the glass equilibrates with alumina, its composition lies within the $CaAl_{12}O_{19}$-$CaO{\cdot}Al_2O_3{\cdot}2SiO_2$-$2CaO{\cdot}Al_2O_3{\cdot}SiO_2$ tie triangle. When the ternary eutectic is reached, anorthite, CA_6, and gehlenite ($2CaO{\cdot}Al_2O_3{\cdot}SiO_2$) are expected to precipitate. This final reaction occurs at below 1400°C.

Glass V/Alumina: At low magnification, Figure III-19, the attack of the glass on the alumina is not very pronounced, particularly in comparison to that exhibited by some of the other glasses. However, closer examination of polished cross sections by optical microscopy shows that the glass has penetrated the alumina. This "swelling" of the alumina due to penetration may offset the alumina removal by dissolution, and thereby produce a nominal glass/alumina interface that differs little in position from that of the original alumina surface.

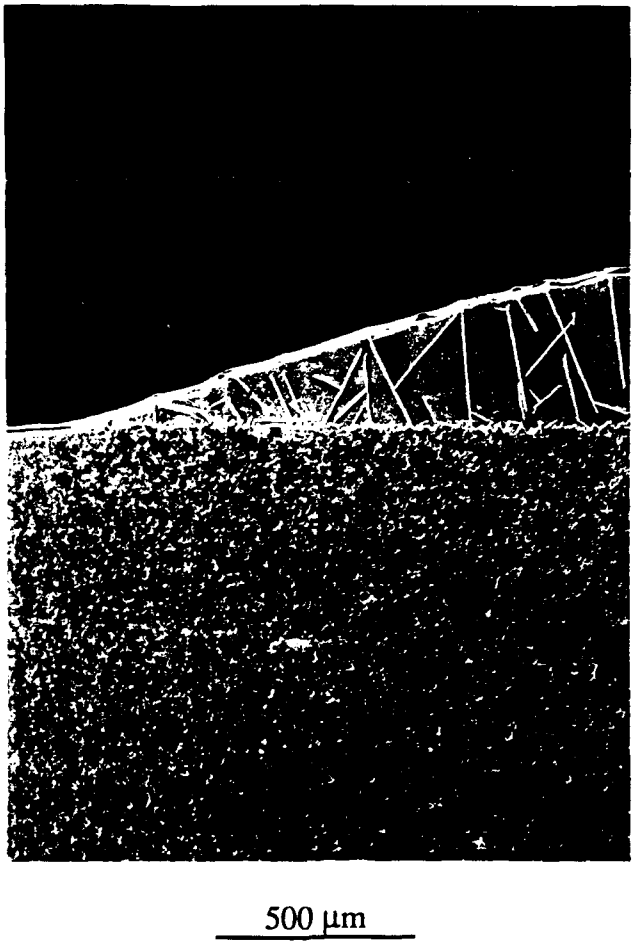

Figure III-19 Low magnification (49X) SEM micrograph of cross section of a sessile drop of Glass V on alumina.

Higher magnification SEM micrographs of the interface, Figure III-20, show that there is at least one crystalline phase, and that there may be two crystalline phases within the glass. One is a platelike particle that appears as a needle in two-dimensional cross sections. X-ray maps indicate that the phase contains primarily aluminum as a cation, and thus, the particle is most likely alumina. This is consistent with the expectation that alumina would be the first phase to form during cooling. There are also packets of platelike particles. No conclusive chemical analysis data for these was obtained, however, we conjecture that these particles are anorthite. The absence of CA6 and gehlenite (as well as the presence of residual glass) may indicate that the resorption of alumina and the formation of these phases is kinetically hindered.

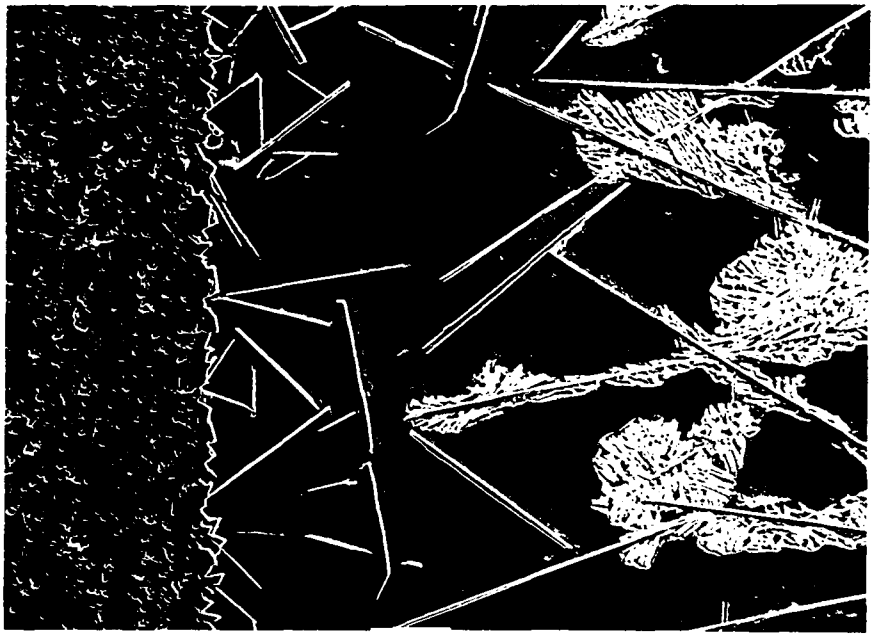

Figure III-20 Higher magnification (100X) SEM micrograph of alumina/Glass V interfacial region and of precipitates in Glass V.

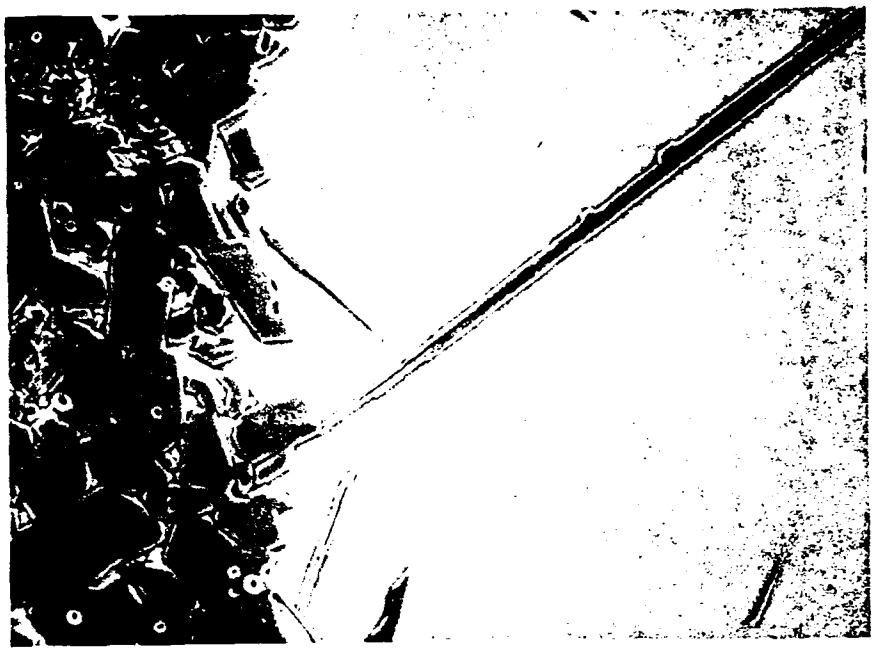

50 µm

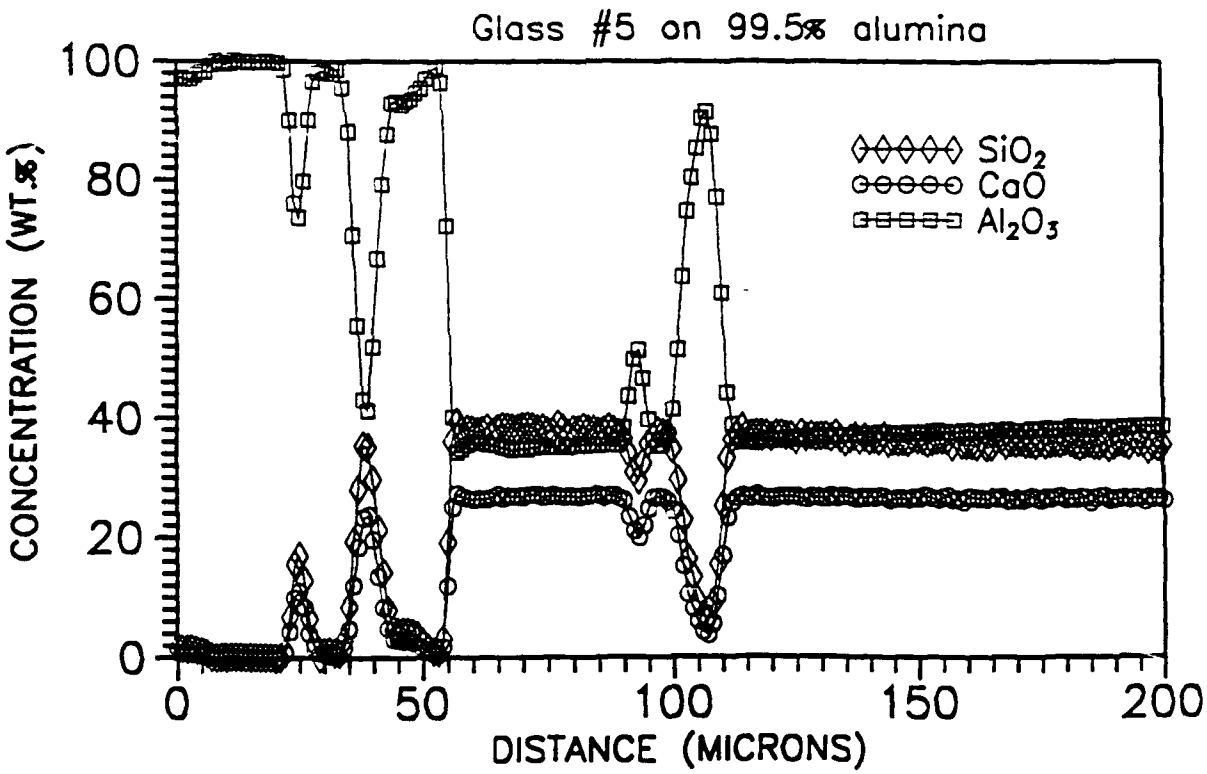

Figure III-21 SEM micrograph (500X) of alumina/Glass V interface, and results of microprobe scan.

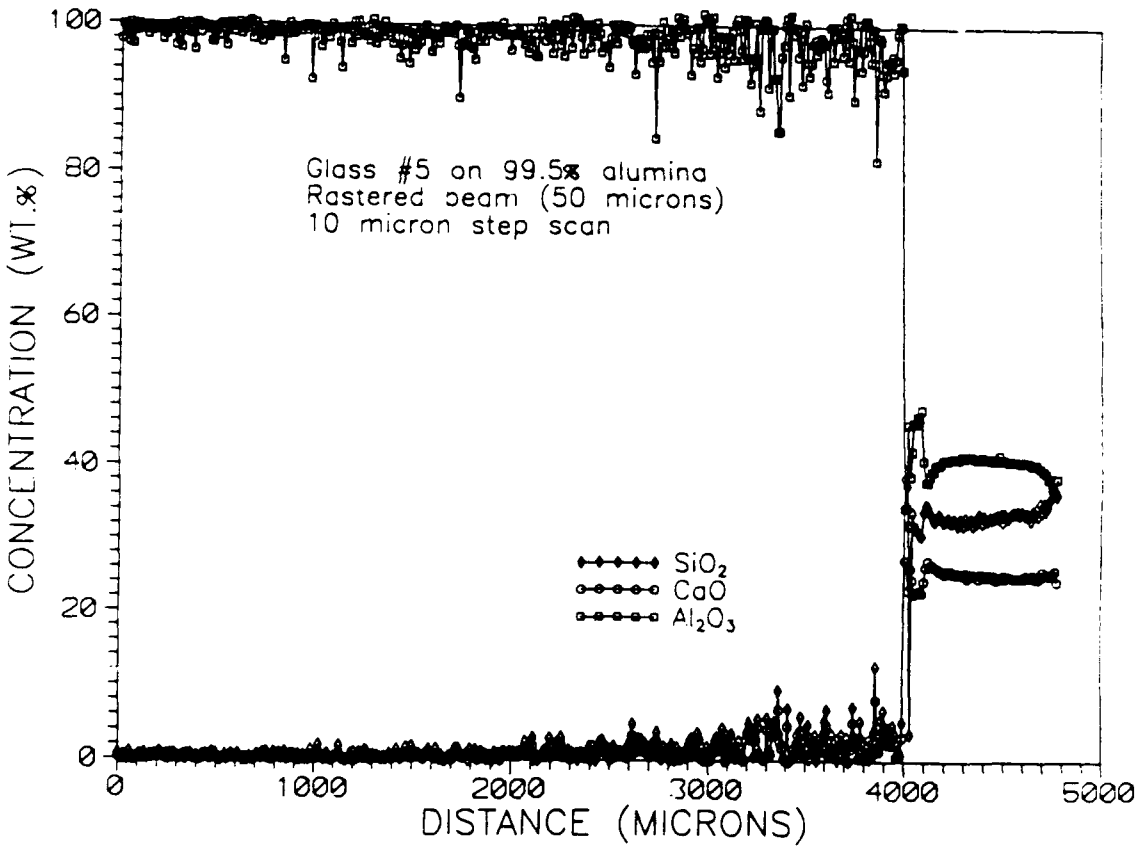

Figure III-22 Results of microprobe scan examining alumina/Glass V interface and glass penetration into alumina.

Glass V/Sapphire: As was the case in Glass V/alumina samples, there is little attack of the substrate by the glass. Some morphological changes are apparent; small ≈10 μm wide sapphire fingers with stairlike surfaces have formed at the interface, as illustrated in Figure III-23. These would be expected to mechanically interlock the glass and substrate. In stark contrast to the microstructures seen in the Glass V/alumina samples, no crystalline phases are apparent.

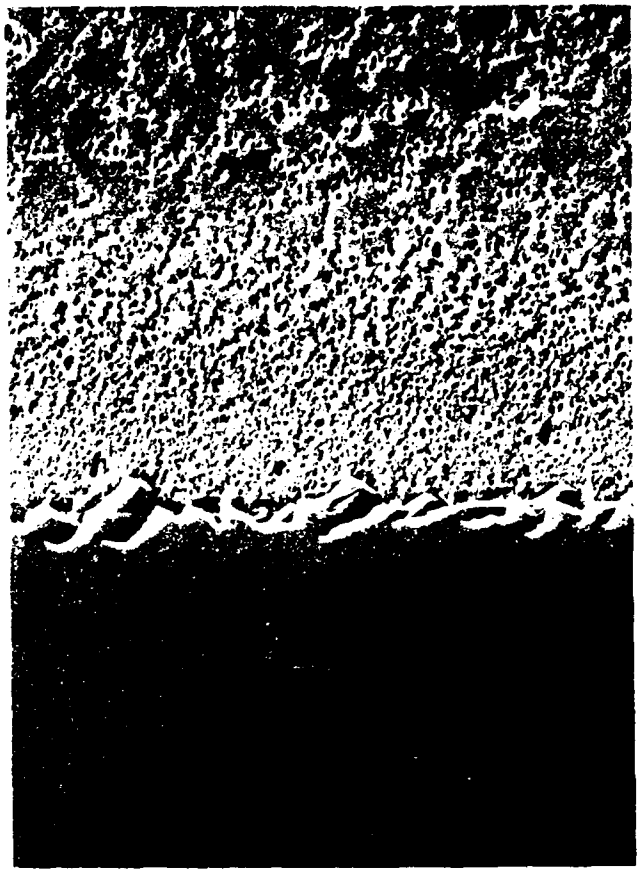

Figure III-23 SEM micrograph (510X) of interfacial microstructure in Glass V/Sapphire sample.

Glass VI (CaO-Al_2O_3-SiO_2-ZrO_2): Glass VI is a quaternary glass from the same system as Glass IV, but with a significantly higher calcia content. As a result, its interaction with alumina, and the nature of the microstructure formed during cooling can be, and were found to be, quite different.

Glass VI/Alumina: Low magnification optical micrographs of the interface show that considerable dissolution of the alumina has occurred. Penetration of glass into the alumina is also suggested. The microstructure within the cooled glass is spatially nonuniform. At the perimeter of the droplet, platelike particles are formed, Figure III-24a. Nearer the center of the droplet, an intertwined "spaghetti-like" structure has developed, Figure III-24b. The cause of this nonuniformity is not known, however, the difference in contact time with alumina between the drop center and the drop perimeter may play a role. At slightly higher magnification, optical microscopy reveals that a precipitate layer has formed along the interface between the alumina and glass.

250 μm

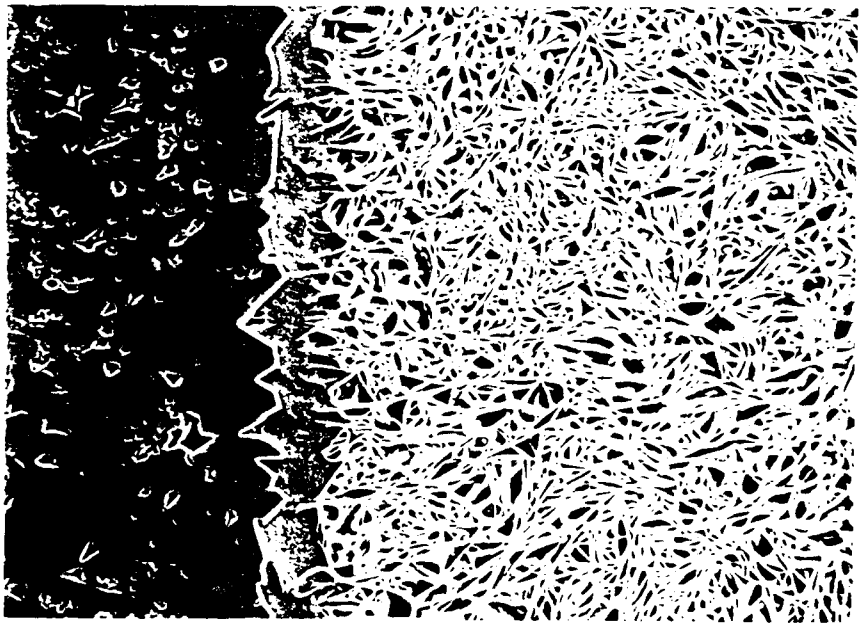

100 μm

Figure III-24 a) Lower magnification (99X) and b) higher magnification (250X) SEM micrographs of alumina/Glass VI interfacial region.

X-ray mapping results shown in Figure III-25 suggest that the interfacial compound contains both aluminum and calcium, with aluminum being the more prevalent cation. EDS results suggest that the interfacial compound is predominantly composed of aluminum (≈87 at %) with the balance of the cations being calcium (≈13 at %). This result, even if not quantitative, coupled with information from the phase diagram, suggests that the interfacial compound may be CA6. Adjacent to this phase is a layer containing relatively higher levels of calcium and silicon, and a substantially lower amount of aluminum. We suspect this is residual glass. The intertwined structure appears to contain all three cations. Qualitatively, calcium, aluminum and silicon are present in decreasing concentration. From the phase diagram for the ternary, one would conjecture that this structure may correspond to gehlenite.

Microprobe scans of the interface were also conducted. The results, and the corresponding micrograph are shown in Figure III-26. Analysis of the region adjacent to the alumina indicates a composition of 91 wt % Al_2O_3 and 9 wt % CaO. This corresponds closely to the composition of CA6 (91.6 wt % Al_2O_3 and 8.4 wt % CaO). The adjacent glass layer has a relatively constant composition, ≈36 wt % Al_2O_3, ≈30 wt % SiO_2, ≈27 wt % CaO, and the balance (≈7 wt % ZrO_2). This composition is close to that of the initial bulk glass. The intertwined phase, tentatively identified as gehlenite, is difficult to evaluate using microprobe analysis. The beam is sufficiently wide that signals from the adjoining glass mix with that from the intertwined phase. X-ray diffraction will be used to identify the phase content of this and other glasses in which uncertainties in the nature of the phases present exists.

In summary, three crystalline phases and a residual glass are present at room temperature. Two of the crystalline phases have been identified. No cracks were evident. Thus, this quaternary glass shows promise, and its potential as a joining material for alumina intended for high temperature applications will be explored.

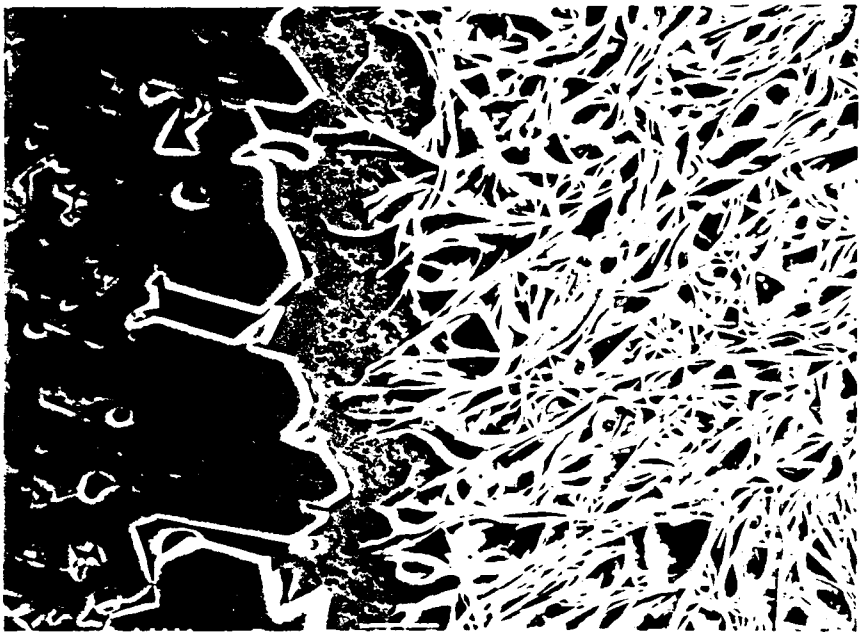

50 μm

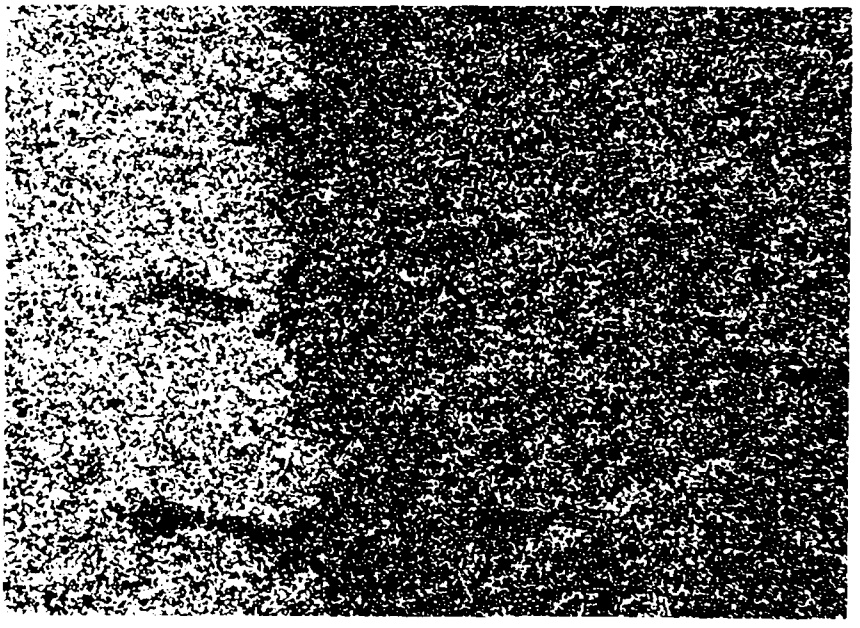

50 μm

Figure III-25 a) SEM micrograph (490X) of alumina/Glass VI interface and b) accompanying x-ray map for aluminum.

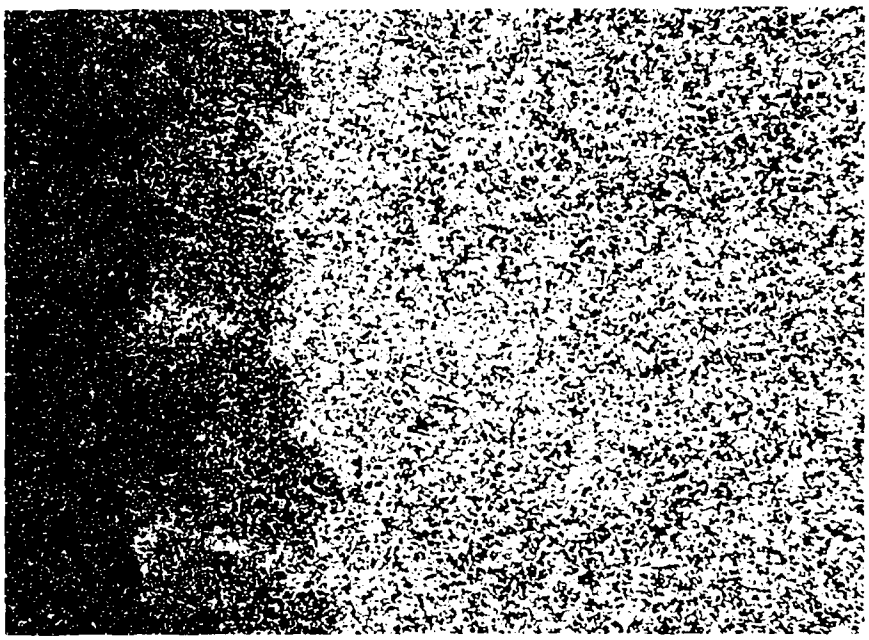

50 μm

50 μm

Figure III-25 (cont.) X-ray maps of c) calcium and d) silicon at alumina/Glass IV interface.

50 μm

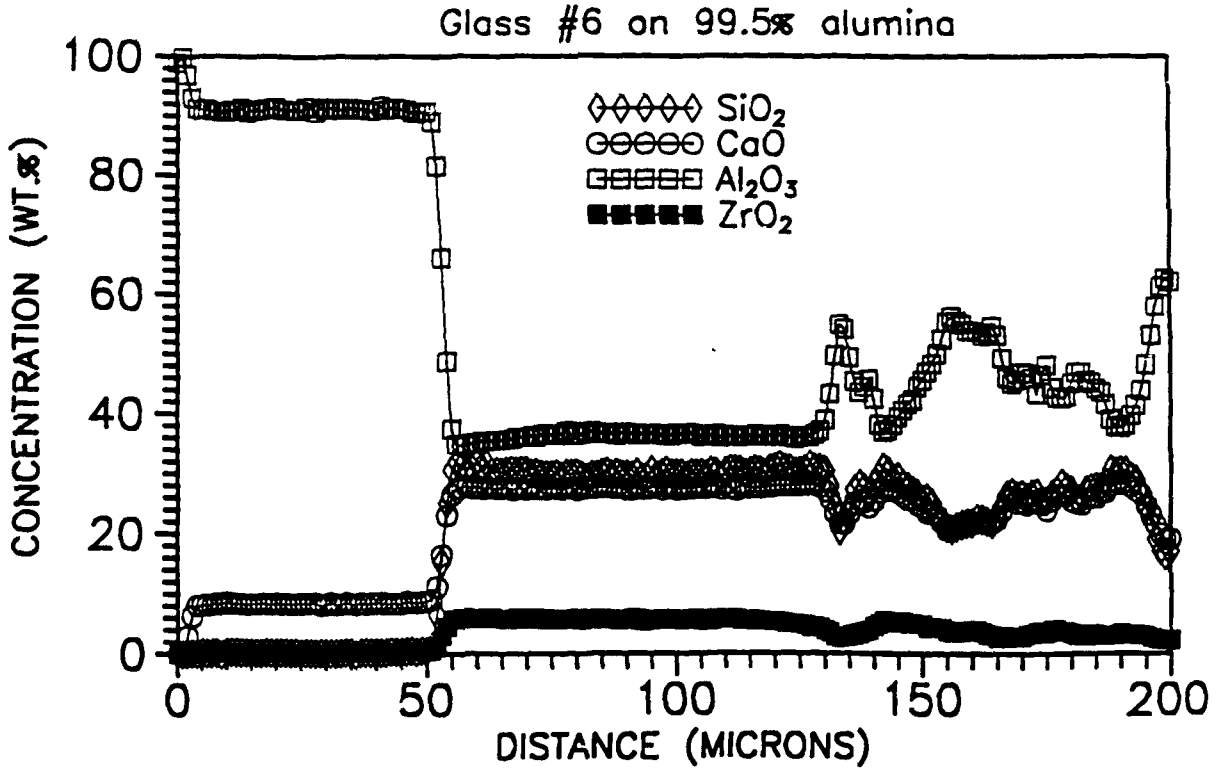

Figure III-26 SEM micrograph (499X) of alumina/Glass VI interface, and results of microprobe scan.

Glass VI/Sapphire: As was the case for the Glass VI/alumina samples, the nature of the phases present in the glass was spatially variable. For Glass VI/sapphire interfaces, no crystalline phases were found at the drop perimeter. Nearer the drop center, a complex microstructure has developed, which incorporates platelike particles, particles with the intertwined structure tentatively associated with gehlenite, and residual glass. Examples of these microstructural features are provided in Figure III-27.

Figure III-27 SEM micrograph (250X) illustrating Glass VI/sapphire interface revealing platelike particles and a phase tentatively identified as gehlenite.

In addition to a complex microstructure within the glass, facetting of the sapphire substrate, and the formation of what appear to be peglike intrusions of the glass into the sapphire is suggested. There is evidence of crystallographic specificity to the orientation of the pegs. This structure is found along the majority of the glass/sapphire interface. In contrast to observations in Glass VI/alumina specimens, there was no evidence for the formation of a CA6 interfacial layer.

Summary and Conclusions

Six refractory glasses were prepared and wetting experiments on alumina and sapphire were conducted. All six glasses were tested with alumina; five were evaluated for sapphire. For the glasses evaluated, liquid formation is not expected until the temperature exceeds 1300°C, and in some cases, until the temperature is well above 1300°C. Wetting experiments on alumina suggest that four of the six glasses should produce crackfree joint regions. A higher sealing temperature may have prevented cracking for the other two glasses. For randomly oriented sapphire, three of the five glasses produced crackfree interfaces. At least three glasses appear suitable for joining alumina to sapphire.

Interfacial microstructures were analyzed using optical and scanning electron microscopy. For selected samples, EDS and microprobe results were used to identify the phases that developed during sealing at 1600°C, and during cooling to room temperature. In all cases, there is residual glass. In most cases, the crystalline phases are consistent with the equilibrium phase diagram, indicating that these diagrams provide a useful tool for selecting and modifying the compositions of glasses for joining applications. At least a subset of these glasses appear to be suitable for joining alumina assemblies intended for high temperature applications.

For some glasses, the microstructures that evolved in glass/alumina and glass/sapphire samples differed. The thermal history was the same for the two samples and is thus not a factor. The microstructural differences may simply be statistical. Alternatively, these differences may reflect the difference in substrate chemistry. Specifically, when an alumina substrate is used, components within the intergranular glassy phase may become incorporated in the glass used for joining. Further work would be required to substantiate this interpretation. However, the implications to joining are important. If thinner glass layers are used, as would be typical in joining, the modifying effect of this form of chemical interaction would become more pronounced. Differences in the alumina used, and the incorporation of different impurities, could transform a glass that is suitable for sealing into one that is not. Finally, with prolonged high temperature use, the potential for chemical and microstructural changes in the joint region exists. Long-term testing is essential.

IV. Joining With Metallic Interlayers:

Introduction

The final approach that was pursued entails the use of metallic interlayers. Although there are many literature references related to solid state bonding, none of them address the specific problem of sealing sapphire to alumina for prolonged operation at 1500°C in the presence of copper vapor. Niobium or platinum (and their alloys) were our first choices for the interlayer material. Both metals bond well with sapphire and alumina and have closely matched thermal expansion coefficients. The effect of alloying additions of several reactive metals (Ti, Zr) on solid state bonding was also determined.

A major concern regarding metal interlayers is chemical compatibility. Once Pt becomes saturated with Cu (at ≈50 at % Cu at 1500°C) a liquid phase forms. For Nb, a liquid phase forms at between 1 and 2 at % Cu. Thus, in the presence of copper vapor, alloying of the bond metal with copper can occur at laser operating temperatures, and ultimately result in the formation of a liquid phase in the bond region. The kinetics of alloying must be determined including the effect of the partial pressure of Cu vapor.

Experimental Procedure

Alloy Preparation

The compositions of metals and alloys which were prepared for solid state bonding joining experiments are presented in Table I. Alloy preparation entailed melting appropriate mixtures of pure metals in a gas tungsten-arc furnace using an argon atmosphere, and then drop casting into a water-cooled copper bar mold. The ingots were cold-rolled to produce 100 μm thick foils for bonding experiments. For the "brittle" alloys it was not possible to fabricate useful foils. For the more ductile alloys, metal foils were cut to the appropriate size, and both faces polished to a 1 μm finish. For Pt foils, the foil thickness was varied (25 μm, 125 μm, and ≈250 μm) to assess the effect of this on bond quality.

Table I Alloy Compositions and Form/Attributes

Metal/Alloy	Description
Pt	Foil
90Pt-10Cu	Foil
97Pt-3Al	Brittle
97Pt-3Ag	Foil
90Pt-10Fe	Brittle
93.5Pt-6.5Ti	Brittle
Nb	Foil
Nb-1Ti	Foil
Nb-2Ti	Foil
Nb-1Zr	Foil
Nb-2Zr	Foil
50Nb-50Zr	Brittle
73Nb-27Pa	Brittle

99.5% pure alumina purchased from Coors, was used. Randomly oriented high-purity sapphire single-crystal wafers were purchased from Meller Optics (Providence, Rhode Island). The as-received 99.5% alumina was cut into plates 22 mm x 22 mm x 3 mm from larger 3 mm thick plates and polished to a 6 μm finish. High-purity sapphire wafers were cut to the same 22 mm x 22 mm x 3 mm dimensions; the wafers are polished to a 0.25 μm finish by the vendor, and were used without additional surface preparation.

For most of the bonding experiments, sapphire/foil/alumina ensembles were placed in a high-purity graphite die. Grafoil™ sheets were placed between the ensemble and the die pistons to accommodate any misalignment. The die was loaded into a vacuum hot press. The system was evacuated until a vacuum of $<5 \times 10^{-6}$ torr was attained. A load sufficient to produce a bonding stress of 15 MPa was then applied and maintained throughout the remainder of the bonding. The press was heated at a rate of 10°C/min to a pressing temperature of 1400°C. The ensemble was held at this temperature for 12 h. The sample was then cooled at ≈10°C/min to 500°C, isothermally annealed at 500°C for 2 h to relieve any stresses that may have been generated, and then cooled at 10°C to room temperature. The applied load was then released.

For platinum/alumina bonding, a wider range of conditions were investigated. A thin Pt foil was placed between two Al_2O_3 surfaces (sometimes precoated with 100 nm of Pt), and exposing the sandwich to a normal compressive stress (≈1 MPa) in an argon atmosphere at ≈0.9 T_m, where T_m is the melting temperature. Three grades of alumina were used in the study; L-Al_2O_3 (96% pure polycrystal); H-Al_2O_3 (99% pure polycrystal); and HP-Al_2O_3 (99.9% pure hot-pressed polycrystal). The aluminas were in the form of 1" cubes. The metal foil thickness ranged between 25 and 250 μm. Flexure specimens were cut from the bonded cubes, the tension faces were polished, and tension edges were bevelled to remove machining flaws. Fracture experiments were subsequently conducted in four point flexure, using a minimum of 12 beams from each bond, and the resulting fracture surfaces were examined in the scanning electron microscope.

Cross-sections of well-bonded specimens were used to assess the interaction between the metallic interlayer and copper. High purity Cu (99.999%) cubes were placed at the interface of alumina/alloy/sapphire cross-section and the ensembles were heated at 10°C/min to 1550°C in a 400 torr argon, held for 50 h, and then cooled at 10°C/min back to room temperature.

Interfacial Characterization

Bonded samples were cut approximately in half using a diamond wafering saw. The sections were mounted and diamond polished to a 1 μm finish. Polished samples were examined using both optical and scanning electron microscopy. Complete cross sections were examined. The degree of bonding defined as the fraction of the total interfacial length along which bonding was apparent was determined from several micrographs for each interface. Samples were also etched to assess the microstructure at and adjacent to the bond interfaces. For Pt-bonded specimens, fracture surfaces were also characterized

Results and Discussion

Platinum and platinum-rich alloys

The three platinum-rich alloys produced an interesting contrast, and forewarned of the potential deleterious consequences of unanticipated chemical interactions between copper vapor and metal interlayers.

Inspection of L-Al_2O_3/Pt and H-Al_2O_3/Pt interface fracture surfaces (Figure IV-1) revealed microstructural defects on the ceramic side in the form of inherent pores. Additionally, while a thin layer of glass covers most of the ceramic surface, regions devoid of glass are presumed to be incompletely bonded, and therefore, microstructural defects. It is presumed that these defects are the fracture origins. Figure IV-1 shows matching fracture regions near the tensile surface of a sample exhibiting a fracture stress of 171 MPa. The glass appears to diffuse from the bulk alumina, "wets" the interface and, at the same time, replicates the alumina grain structure on the metal side. X-ray Photon Spectroscopy (XPS) of L-Al_2O_3/Pt fracture surfaces revealed the presence of Pt, Si, SiO_2, Na and Ca on the Pt side, and on the Al_2O_3 side, O, Al, Si, Pb, Ca, and Na, with the Si/Al ratio decreasing rapidly with profiling depth.

SEM observations suggest that the glass is drawn to the Al_2O_3/Pt interface. The left hand side of Figure IV-2a shows an area of Al_2O_3 that was not in contact with Pt during diffusion bonding, i.e., a free surface (achieved by indenting the Pt foil prior to bonding). In this region, grain surfaces and boundaries are clean compared with the adjoining region. The surface glaze is shown at higher magnification in Figure IV-2b. Additionally, the white regions on the free surface which form by the disruption of the original Pt precoat are also underlayed with glass. Transmission electron microscopy (Figure IV-3) confirmed the presence of a thin amorphous phase at L-Al_2O_3/Pt and H-Al_2O_3/Pt interfaces.

HP-Al_2O_3/Pt interface fracture surfaces revealed a theoretically dense fine-grained (≈3 μm grain size) ceramic surface, and distributions of voids on the metal side which derive from incomplete diffusion bonding. Again, these defects are presumes to be the fracture origins. Indeed, when short bonding times, i.e., up to 4 h, were employed with the HP-Al_2O_3, low stress fracture occurred (see Figure IV-4), and subsequent SEM examination revealed large unbonded areas near the beam tensile surface on the metal side.

Strength tests indicated that all bonds exhibit essentially linear behavior prior to fracture. The highest strengths typically corresponded with failure originating within the Al_2O_3. Otherwise, fracture occurred at the interface.Mean strength values are plotted in FIgure IV-4; the values for HP-Al_2O_3 are included for completeness and to illustrate that the absence of silicate impurity requires that extended soak times be employed to achieve significant bond strength. The mean strengths of the L-Al_2O_3 and H-Al_2O_3 were also determined for reference. It is apparent that interfacial failure is sensitive to the metal layer thickness, whereas failure in the ceramic is essentially thickness independent. Ceramic failure was observed in some specimens with metal thickness up to 125 μm. The prior finish on the ceramic contact surface also appears to influence failure, especially for bonds with the thinner metal layers. This is also supported by the Weibull plots of failure probability in Figure IV-5, which show the strength data obtained for L-Al_2O_3/Pt bonds having metal thickness 75 μm. However, the significant variable is clearly bonding time, the plot for specimens bonded for 2 h having similar characteristics to those for the ceramic reference.

Two Pt-rich alloys were also tested, and the results indicate the importance of metal interlayer chemistry. Neither alloy proved to be satisfactory. The sapphire/alumina ensemble joined with 97Pt-3Ag was bonded following removal from the hot press. During preparation of

Pt/Al2O3 Fracture Surfaces
(171 MPa)
Pt
Al2O3
alumina
platinum
30 μm

Figure IV-1

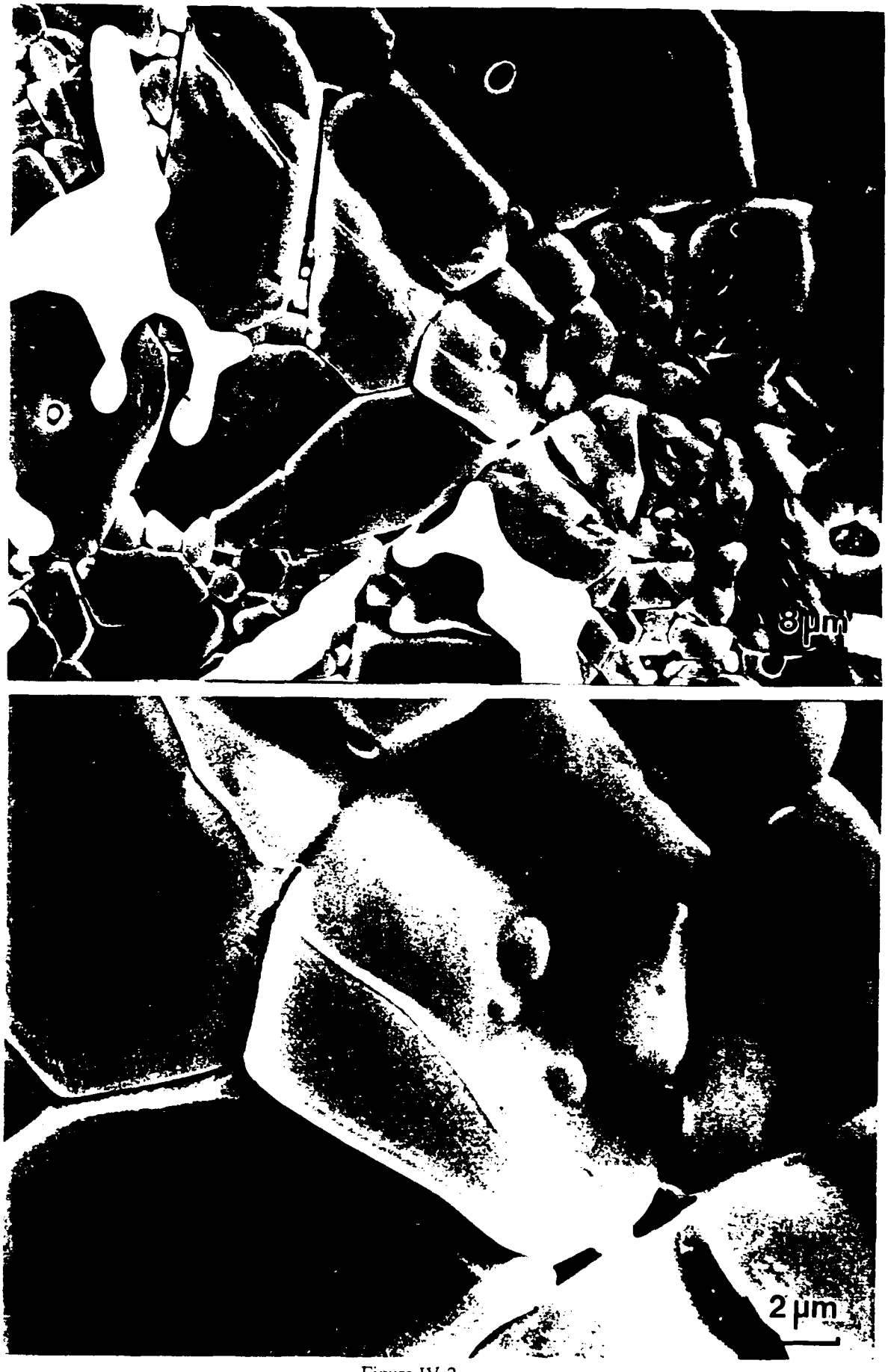

Figure IV-2

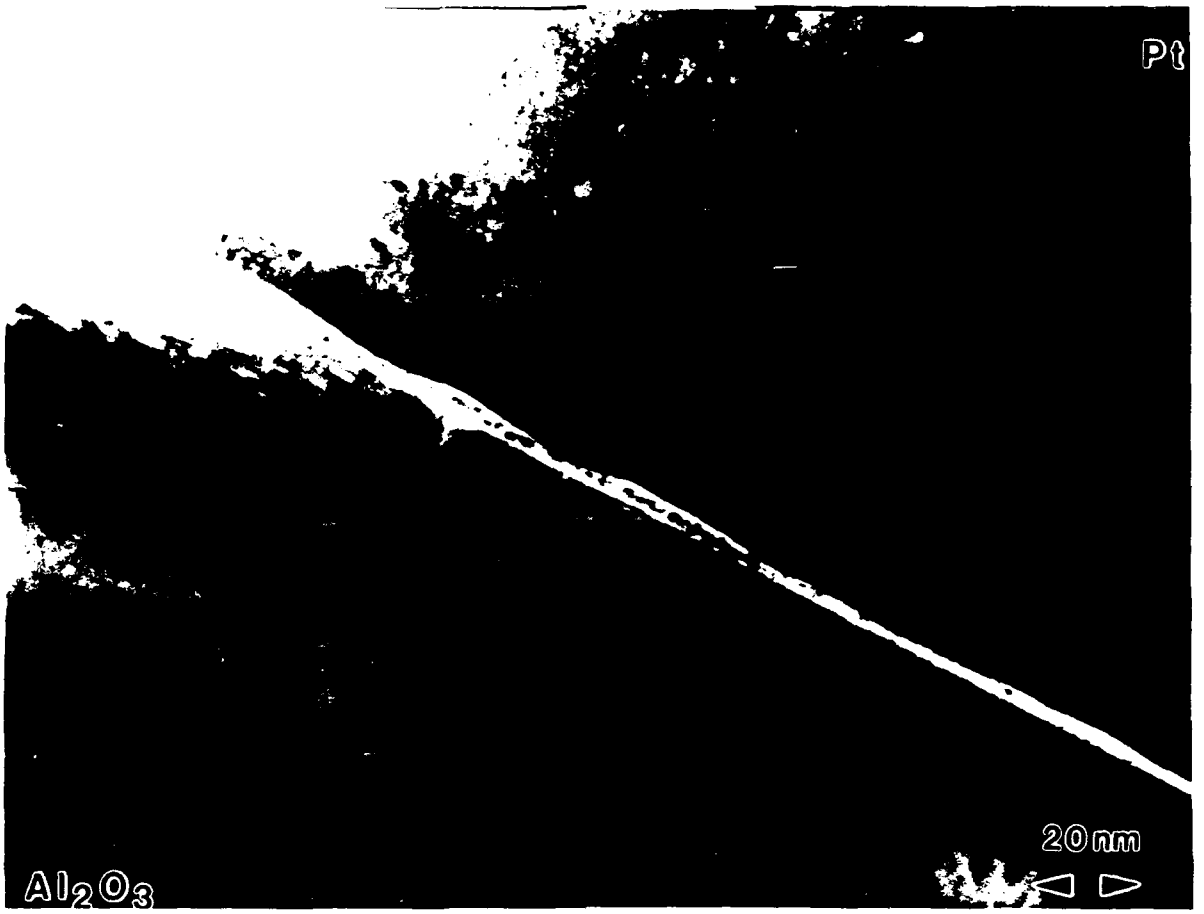

Figure IV-3

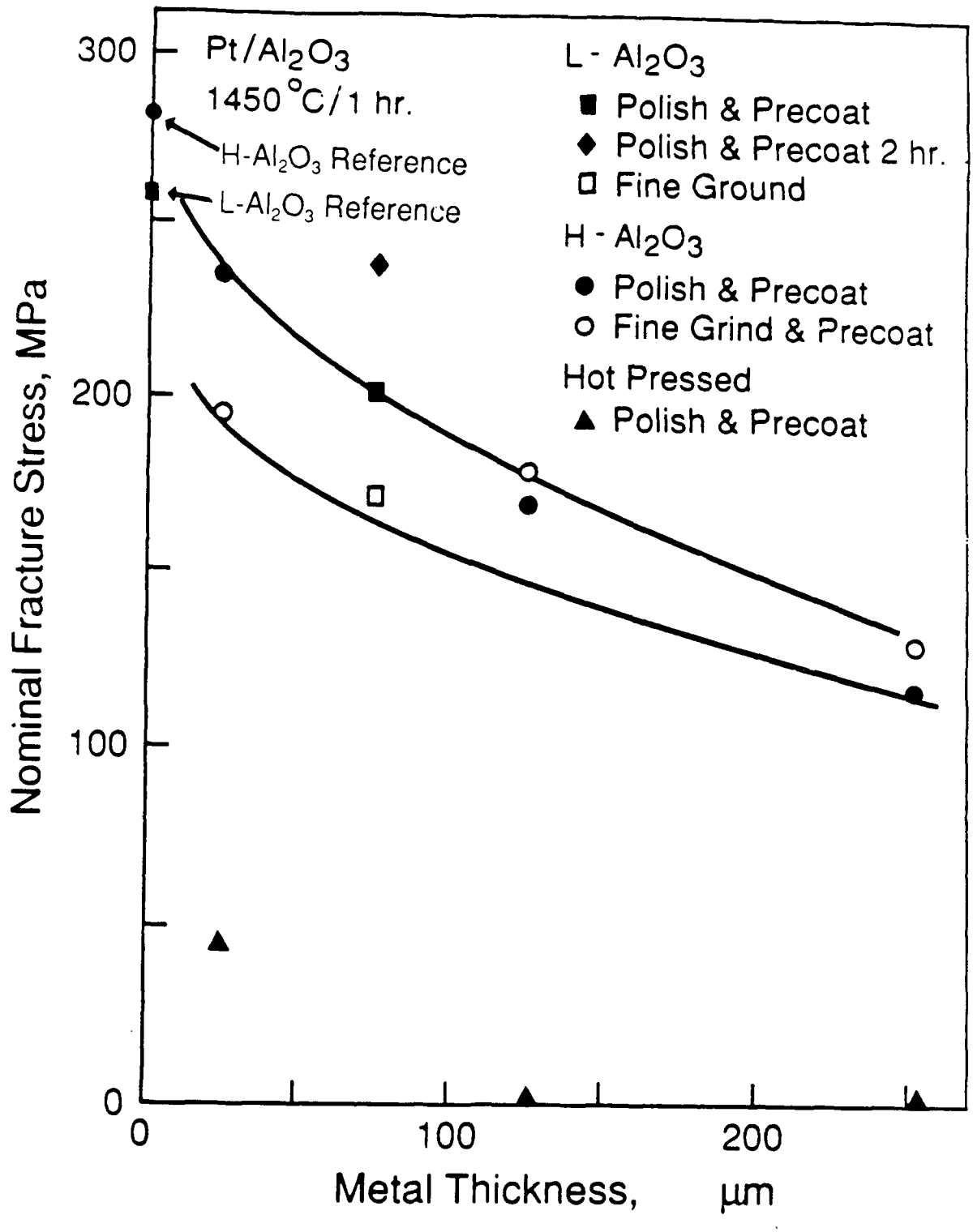

Figure IV-4 Nominal fracture stress versus Pt foil thickness. The effects of alumina purity and sample surface preparation on bond strength were also explored.

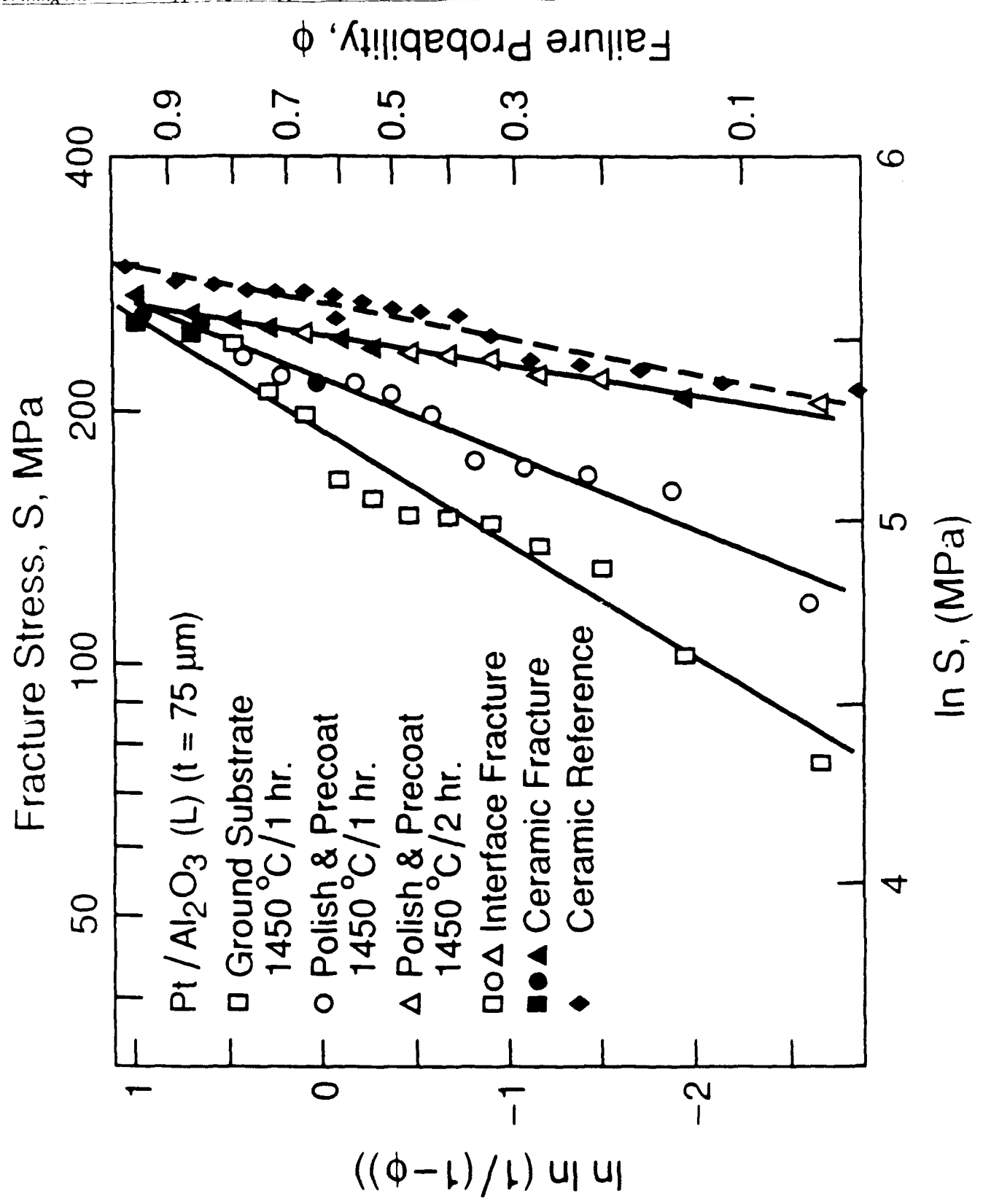

Figure IV-5 Strength data for samples joined with a 75 μm thick Pt foil as a function of surface preparation and bonding time

cross sections, some separation of the foil and ceramic occurred. The foil separated easily from the sapphire. With light pressure, the foil could be peeled from the alumina. These observations suggest that only weak adherence developed. The relatively stronger adherence of the foil to the alumina may be the result of reaction with the glassy phase in the alumina, intrusion of the metal into the pores of the alumina (see Figure IV-6), or a combination of the two effects. For the 90Pt-10Cu alloy, little or no adherence developed. When the sample was removed from the hot press, the sapphire separated without any applied force. The foil separated easily from the alumina. Again, mechanical interlocking due to intrusion of the alloy into the surface pores of the alumina may be the primary difference between the two interfaces.

These effects of alloying on bond strength indicated by these results have important implications. As we anticipated, they demonstrate that relatively modest changes in interfacial chemistry may be sufficient to result in a significant degradation in joint strength. Specifically, the results indicate that exposure of a platinum foil bonded ensemble to copper vapor could have deleterious effects on strength. Apparently, at Cu contents below 10%, a complete loss of adherence occurs. In a bonded ensemble, one would expect the exposed inner seal surface to weaken first. Localized loss of adherence would create a flaw and assist in bringing additional copper vapor to the Pt/alumina or Pt/sapphire interface. If metal interlayers are to be used, chemical interactions between metallic interlayers and copper vapor must be considered, and the timeframe for chemical degradation and failure must be quantified. Initial work addressing this issue is provided in an ensuing section. More extensive work of this type would be conducted as part of Phase II research.

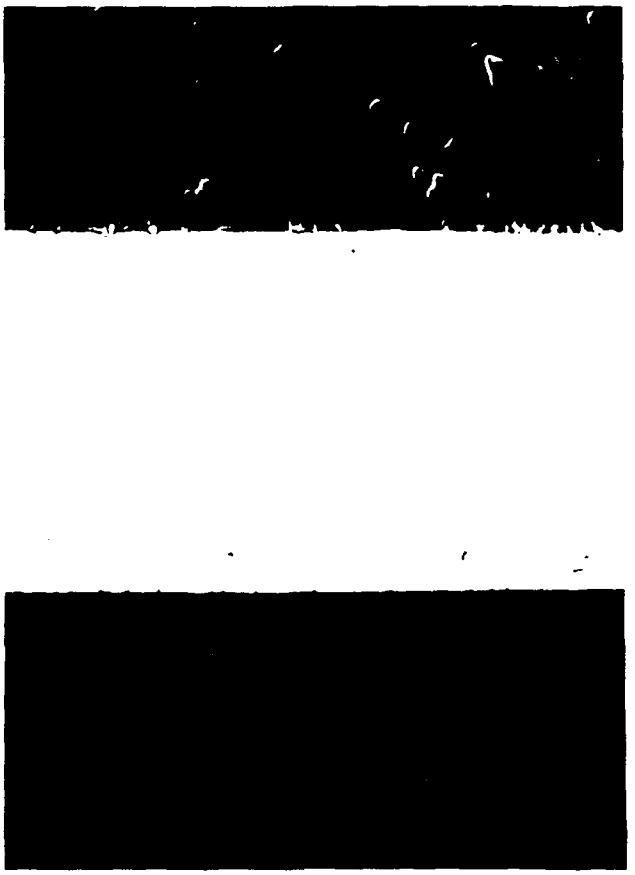

Figure IV-6 SEM micrograph of (top to bottom) alumina, 97Pt-3Ag, and sapphire. Note the intrusion of the metal into the open pores of the alumina.

Niobium and Niobium-rich alloys

The results for all five niobium or niobium-rich alloy interlayers were similar; a well-bonded nearly defect-free interface resulted. None of the specimens underwent separation during handling or preparation of cross sections. Those defects that are present typically have a size that is no larger than that of the larger pores in the alumina. Thus, although there are interfacial defects, they are not the result of incomplete bonding. Figure IV-7 typifies the quality of the joint interface that was obtained for all five alloys; the specific interface shown is for a 99Nb-1Ti alloy.

EDS line scans of interfaces between titanium-doped niobium alloys indicate that Ti interacts with silicon in the glassy phase of the alumina to produce precipitates that contain Si,Ti, Al, and Nb as cations. These precipitates form within a layer up to 10 μm from the alumina/alloy interface. At the foil/sapphire interface, no evidence of reaction is found. EDS line scans of interfaces between zirconium-doped niobium alloys showed no comparable precipitate formation. The 99Nb-1Zr alloy was unique in that roughening of the sapphire surface is evident, possibly indicative of the formation of a reaction layer. Further study of this is required. .

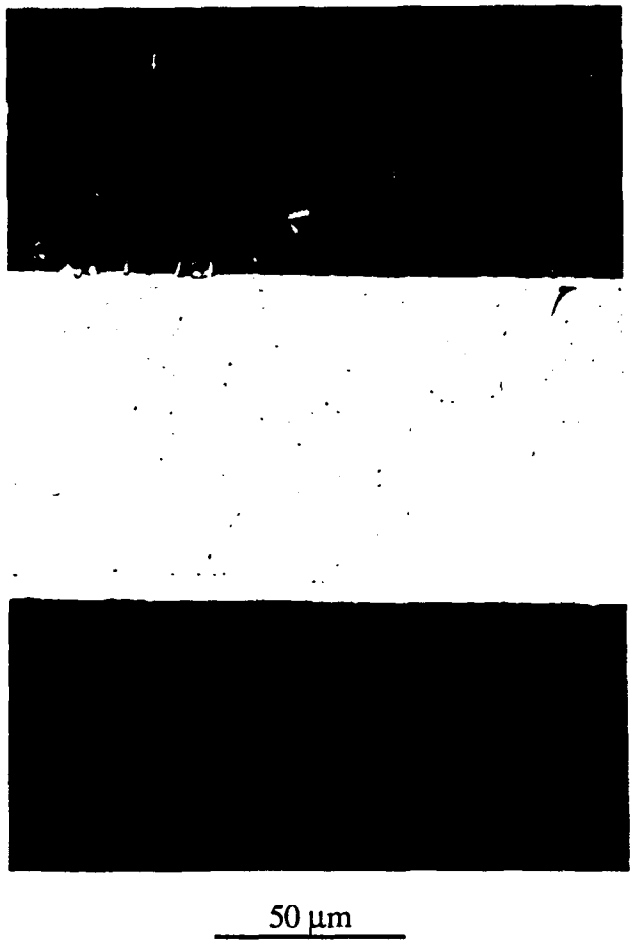

Figure IV-7 SEM micrograph of (top to bottom) alumina, 99Nb-1Ti, and sapphire. The degree of bonding is typical of that achieved for all niobium and niobium-alloy foil bonded specimens.

Interactions Between Metal Interlayers and Molten Copper

As discussed in the Phase I proposal, and demonstrated by the results with platinum-based foils, small changes in chemistry can dramatically impact the bond strength. To obtain some information on the susceptibility of metal interlayer bonded ensembles to degradation via chemical interactions with copper, well-bonded samples were cut, a copper cube was placed at the joint, and the sample was annealed for 50 h at 1550°C in a 400 torr argon atmosphere to suppress vaporization. The results were dramatic.

For alumina/sapphire ensembles bonded with platinum and with 97Pt-3Ag foils, the bond totally disintegrated. Alloying with copper apparently creates volatile species. In both cases, there was little if any evidence for residual metal at the sapphire/alumina interface. These findings should cause considerable doubt as to the suitability of platinum or platinum alloy bonds for high temperature use in copper vapor lasers.

The results obtained with niobium and niobium alloy bonded couples were less dramatic, but the source of no less concern. Viewed through the sapphire, a several mm penetration depth of

copper into niobium is readily detectable. We suspect that this region of the sample was molten at the anneal temperature.

There are important differences between the experiment conducted, and actual operating conditions in the laser. In the present case, there is direct contact between liquid copper and the metallic interlayer. As a result, the physical concentration of copper is substantially higher than it would be in the case of contact with a vapor. However, since the copper vapor is nominally in equilibrium with liquid copper, the chemical potential, and thus, the thermodynamic driving force for alloying should be identical, or in the case of a slightly lower copper pressure, similar to that tested in the present experiment. We emphasize that our test was only of 50 h duration, and the intended lifetimes of the laser systems are presumably several thousand hours. The findings thus raise doubts about the suitability of niobium-bonded laser assemblies. Further testing is clearly necessary.

Summary:

Four distinct approaches to bonding alumina to sapphire and alumina to alumina were investigated: 1) solid-state or **direct** joining, 2) use of glass-bonded alumina interlayers, 3) joining with a devitrifiable **glass**, and 4) use of a **metallic** (Nb or Pt or their alloys) interlayer. Each approach has advantages and disadvantages. The experience we have gained from the Phase I research and independent closely related studies has helped to define conditions that produce (or in the case of sealing with glasses, should produce) viable seals, and identified the key issues that need to be addressed in Phase II studies.

The experiments have demonstrated an ability to bond a 1" by 1" sapphire wafer to polycrystalline 99.5‰ alumina by vacuum hot pressing (1400°C, 15 MPa, 12 h, $<5 \times 10^{-6}$ torr). A sapphire/alumina interface that is essentially free of bonding defects was produced. Five thermal cycles between 800°C and 1550°C produced no observable degradation in bond quality. Considerable care in producing flat and polished surfaces is required. However, from the standpoint of chemical compatibility, this type of joint/seal is the most desirable. Mechanical characterization of alumina/sapphire/alumina bonds should be performed to assess the strength of the joints at elevated temperature.

Glass-bonded alumina interlayers were used to bond high purity alumina to sapphire. By bonding at 1700°C (even with negligible load) pore-free sapphire/95% alumina interfaces were produced. With greater emphasis on surface preparation and improved methods of applying stress during bonding, we anticipate that higher-quality alumina/alumina interfaces, e.g., better than 72‰±18‰ could be achieved at lower bonding temperatures. The creep and fracture characteristics of the glass-bonded alumina used are not known. Mechanical properties of both the glass-bonded alumina, and joints prepared with the alumina should be determined as a function of temperature. The potential for increasing the viscosity and reducing the creep rate of the glass bonded alumina by post-joining heat treatments makes joining with glass-bonded aluminas an attractive approach that merits further study.

Six refractory glasses were prepared and wetting experiments at 1600°C on alumina and sapphire were conducted. All six glasses were tested with alumina; five were evaluated for sapphire. Wetting experiments on alumina suggest that four of the six glasses should produce crackfree joint regions. A higher sealing temperature may have prevented cracking for the other two glasses. For randomly oriented sapphire, three of the five glasses produced crackfree interfaces. Thus, at least three glasses appear suitable for joining alumina to sapphire. Bonded specimens need to be produced and evaluated.

Of the thirteen metallic and metallic alloys that were prepared, eight produced foils suitable for joining studies. High purity Pt foils, and foils from two Pt-rich alloys were studied. Although pure Pt produced strong bonds, alloying led to severe reductions in adhesion and bond strength. Pure Nb foils, and foils prepared from four alloys of Nb with reactive metals were examined. All Nb foils produced strong defect-free bonds. Joints produced using the alloys that produced well-bonded strong ensembles, were exposed to liquid copper for 50 h at 1550°C. The results raise serious doubts about the use suitability of metallic interlayers for producing sealed copper vapor lasers. Further testing would be required to assess the degree of alloying between copper vapor and the interlayers during prolonged exposure.

References

1. J. Collyear, "A programe for the wider application of new and improved materials and processes", HMSO, 1985.

2. J. Rödel and A. M. Glaeser, "Production of Controlled Morphology Intergranular Pore Arrays: Implications and Opportunities," J. Am. Ceram. Soc., 70, [8], C172-C175 (1987).

3. J. Rödel and A. M. Glaeser, "Application of controlled interfacial pore structures to kinetic studies in alumina," to appear in Interfacial Structures, Properties and Design, (Mater. Res. Soc. Proc., 122, Pittsburgh, PA 1988).

4. M.G. Nicholas and D.A. Mortimer, "Ceramic/Metal Joining for Structural Applications," Mat. Sci. & Tech. 10, 657-665 (1985).

5. K. Suganuma, Y. Miyamoto and M. Koizumi, "Joining of Ceramics to Metals", Ann. Rev. Mater. Sci., [18] 47-73 (1988).

6. J.T. Klomp, "Ceramic-Metal Reactions and Their Effect on the Interface Microstructure," Presented at "Ceramic Microstructures '86: Role of Interfaces" Conference at the University of California in Berkeley July 1986.

7. J. T. Klomp, "Bonding of Metals to Ceramics and Glasses", Am. Ceram. Soc. Bull., 9 [51] 683-688 (1972).

8. S. M. Wiederhorn, B. J. Hockey, R. F. Krause and K. Jakus, "Creep and fracture of a vitreous-bonded aluminium oxide," J. Mater. Sci., 21, [3], 810-24 (1986).